The Pennsylvania State University

The Graduate School

Department of Materials Science and Engineering

REINFORCEMENT OF NATURAL RUBBER LATEX BY NANOSIZE MONTMORILLONITE CLAY

A Thesis in

Materials Science and Engineering

by

Rattana Tantatherdtam

Submitted in Partial Fulfillment
of the Requirements
for the Degree of

Doctor of Philosophy

August 2003

The thesis of Rattana Tantatherdtam has been reviewed and approved* by the following

Ian R. Harrison

Professor of Polymer Science

Thesis advisor

Chair of Committee

Paul R. Howell

Professor of Metallurgy

Sridhar Komarneni

Professor of Clay Mineralogy

James P. Runt

Professor of Polymer Science

Graduate Program Coordinator

Department of Materials Science and Engineering

* Signatures are on file at the Graduate School

ABSTRACT

Based on the unique character of montmorillonite namely its layer structure and the ability of silicate particles to separate into nanometer-size platelets, natural rubber (polyisoprene)/ clay composites were obtained by mixing rubber latex with clay-water dispersion and coagulating the mixture. The resulting film had greatly improved mechanical properties compared with films using micron-sized fillers. Further, both modulus and toughness were improved; in many composite system an improvement in modulus leads to a loss of toughness. X-ray diffraction results indicated that clay platelets dispersed in the rubber matrix on the nanoscale level with some macromolecules intercalated into the clay gallery. The observed considerable improvement in mechanical properties, coupled with a theoretical model of composite modulus suggests a dispersed structure of clay in the composite. While not all clay particles are exfoliated, data suggest that a reasonable fraction of exfoliated materials is required to explain the experimental results.

Table of Contents

List of Figures

List of Tables

ACKNOWLEDGMENTS

I would like to express my gratitude to my advisor, Dr. Ian R. Harrison for his guidance and encouragement throughout this work. His generosity, patience and sense of humor have always been admired.

Many thanks go to Dr. James P. Runt, Dr. Paul R. Howell and Dr. Sridhar Komarneni for serving as my committee. I would also like to thank my friends in the IRH group: Nandh Thavarangkul, Claudia Alencar Fonseca and John Chen who gave me a helpful advice not only in research problems but also in life. In addition, My study life here will never be warm, enjoyable and memorable without you guys, Atitsa Petchsuk, Pakorn Opaprakasit, Cattleya Kongsupapsiri, Ratda Suhataikul, Chuttchaval Jeraputra, Wallop Promsen and Mantana Kanchanasopa. It is the Thai Student Association here at Penn State that keeps us as a warm community that I never expected far away home. I should not miss to mention several friends at home whose love and support are overwhelmed.

Furthermore, the financial support from the Royal Thai Government, NSF and the opportunity given by Polymer Science Program, PSU are truly appreciated.

Finally, I am indebted to my parents, whose unconditioned love and care to this "little girl" has never been far away. Their 'brave heart' pushed me through all the difficult times and inspired me to pursue my dream.

CHAPTER 1

INTRODUCTION

1.1 Thesis motivation

Natural rubber is an important material used in a wide assortment of engineering applications. Its use depends mainly on its inherent soft and highly deformable nature. However, fillers are incorporated in order to modify certain properties to an acceptable level. The choice and level of loading of filler depends primarily on the particular product and its vulcanizate properties. Filler systems are composed of a variety of materials including carbon black, mineral products such as kaolin (or china clay) and calcium carbonate. Clay is one of the most widely used nonblack fillers for rubber. Clay is an inexpensive natural mineral and has been an important part of the rubber industry where it is used as economical filler to modify processing and performance of natural and synthetic rubbers. There are many types of clays, but kaolinite has long been reported to be the most important inorganic filler incorporated into natural rubber latex [1-3].

In the past, where reinforcement of the polymer was not the main factor, different types of clay minerals have been used as fillers to reduce the cost of the host polymer and provide certain properties useful in rubber compounding. The term "reinforcement" refers to an improvement in end use performance of the rubber compound associated with an increase in modulus and in the so called ultimate properties including tensile strength, tear resistance and abrasion resistance. It has been well known that particle size, structure, and surface characteristics of reinforcing materials were three factors that

influence and help decide their reinforcing ability, and of these factors particle size of the filler has the most significant influence [4-8]. In general the reinforcing ability of clay is considered to be poor because of its large particle size and low surface activity, although clays have a long tradition as semi-reinforcing fillers and extenders in the plastic industry.

Recently, the 2:1 phyllosilicates have attracted a great deal of interest as nanocomposite reinforcements in polymers owing to their intrinsically anisotropic character and swelling capabilities. Moreover, these materials posses a high aspect ratio (500-2000) and a plate-like morphology. Because of the clay layer structure and its ability to disperse into nanometer-size platelets, nanometer reinforced materials with unique physical and chemical properties have been obtained. It has been reported in the literature that exfoliated structures are primarily responsible for high mechanical reinforcement, while intercalated structure having a smaller aspect ratio play only a minor role [9,10].

So far montmorillonite clay claims the most attention due to its ability to show extensive interlayer expansion or swelling. In a pristine state, interlayer cations which are usually Na^+ or K^+ ion can be exchanged in solution for other species. This property results in their expandability in water and aqueous electrolyte solution [11]. These characteristic therefore could provide a way to prepare clay composite in a watery rubber latex form.

1.2 Research approach

A variety of clays have recently been used to obtain nanocomposites by exploiting the ability of clay silicate layers to be dispersed into polymers at the nanoscale level. Montmorillonite clay was selected as the filler in a study of natural rubber latex composites. Montmorillonites are relatively cheap materials with fine-grained particle and high surface area. In addition, they are readily dispersed in water (latex) without the aid of dispersing agents and are easily incorporated as a dry or aqueous dispersion without risking the destabilization of the latex. The crystal structure of the clay itself is most important. The characteristic expansion of the interlayer structure exposes a large active surface area and permits polymer molecules to enter into the galleries. Separation of clay platelets can occur under certain conditions giving a very high aspect ratio filler which dramatically improves composite properties.

Differences in behavior between kaolinite and montmorillonite clay stem from their composition and structure [2,4,11]. Kaolinite has an idealized chemical composition of $Si_2Al_2O_5(OH)_4$. Its structure consists of a gibbsite $Al(OH)_3$ layer bonded to a siloxane (Si_2O_5) layer. In contrast montmorillonite has one gibbsite layer interposed between two silicate sheets. The successive pairs of layers of the kaolinite structure are held together by hydrogen bonds which are relatively strong, whereas successive layers of montmorillonite structure are held by electrostatic and weak van der Waal forces. Consequently, montmorillonite has the ability to undergo extensive interlayer expansion or swelling in a direction perpendicular to the silicate anions. On the other hand, only very limited swelling is possible in the case of the firmly bonded kaolinite structure.

So far there has been no investigation on the use of nanolayered silicates in a natural rubber latex system. Therefore, the present study represents an attempt toward introducing nanolayers of montmorillonite clay into natural rubber (cis-1,4-polyisoprene). The primary interest is to determine the effect of these fine particle clays on the mechanical properties of the resulting composite elastomer. We imagine that the reinforcing capacity of montmorillonite in the resulting dried latex film would be enhanced by the fact that the rubber latex particle is coated with protein layers, which behave as a hydrophilic colloid to which montmorillonite as another hydrophilic colloid is added, therefore allowing an improved dispersion of clay in the latex system.

The current study has been carried out in two directions. First, the influence of expandable clay, montmorillonite, on the properties of natural rubber obtained from unvulcanized latex film was investigated. Second, the reinforcing effect obtained by the introduction of layered silicate filler was examined using x-ray diffraction (XRD) method in an attempt to understand any observed property improvements on a nano or molecular level.

1.3 Natural Rubber

Today more than 80% of the total world production of natural rubber comes from southeast Asia. Malaysia is the largest producer, followed by Indonesia. Thailand accounts for much of the remainder in this area [12]. Rubber is collected in the form of latex that exudes from the bark of the tree when it is cut. The average rubber content of latex may range between 30-45%. This fresh 'field' latex is not utilized in its original

form due to its high water content and susceptibility to bacterial attack. It is necessary both to preserve and concentrate the latex, so that the end product is stable and contains 60 % or more of rubber. Latex concentrates are differentiated by the method of concentration, and type of preservative used. Concentration is achieved by centrifugation (most common), by creaming, or by evaporation. Currently, about 50% of all latex concentrate is consumed by the dipped goods industry (medical and household gloves). Other uses of latex are in carpet backing, thread and adhesives.

1.3.1 Chemical structure

Natural rubber is a high molecular weight polymer of isoprene, C_5H_8. The repeating unit is –CH–C(CH3)=CH–CH2– . Hevea rubber which is extracted from the tree *Hevea Brasiliensis* is the major naturally occurring form of 1,4-polyisoprene. This rubber contains more than 98% of its double bonds in the cis configuration which is essential for elasticity in polyisoprene. Over 90% of all cis -1,4-polyisoprene used industrially is natural Hevea rubber [13].

1,4 polymerization of the conjugated diene system of isoprene leads to a polymer structure with a repeating alkene double bond in the polymer chain (I)

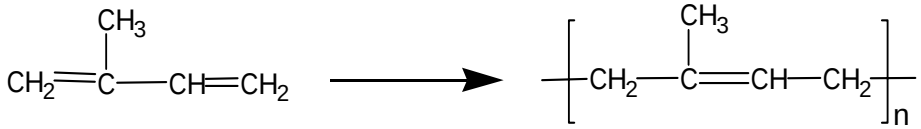

(I)

The double bond in each repeating unit in the polymer chain is a site of steric isomerism since it can have either a cis or a trans configuration. The polymer chain

segments on each carbon atom of the double are located on the same side of the double bond in the cis configuration (II) and on the opposite sides in the trans configuration (III).

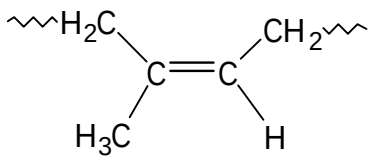

Cis

(II)

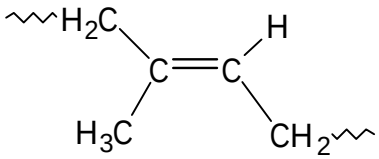

Trans

(III)

Stereoisomerism in 1,4-plyisoprene results in significant differences in the properties of the cis and trans polymers. The trans isomer which has a higher molecular symmetry crystallizes to a greater extent and therefore has higher T_m and T_g values. cis-1,4-polyisoprene has very low crystallinity, low T_m and T_g values, and is an excellent elastomer over a considerable temperature range. Trans-1,4-polyisoprene is a much harder, much less rubbery polymer since it has relatively high T_m and T_g values and significant crystallinity. It is less an elastomer and more like a thermoplastic. 1,4-Polyisoprene is found in nature in both the cis and trans forms.

1.3.2 Latex properties

Natural rubber latex basically consists of a dispersed phase containing rubber particles (poly-cis-1,4- isoprene) and other non-rubber components in minor quantities, and the dispersing medium, water, which contains several organic substances and mineral salts. Rubber particles are formed by aggregation of molecules of rubber hydrocarbon

and overall have a spherical, oval, pear-like and various other constricted forms [7]. Particle sizes range from 0.1 to 4 μm. These latex particles are stabilized by the presence on their surfaces of absorbed carboxylic anions from fatty acid soaps and protein molecules. The absorbed anions cause the particle surface to have a net negative electrical charge which produces inter-particle repulsive forces and hence ensures absence of aggregation and stability of the latex.

Natural rubber latex concentrates are highly specified materials and are characterized by a number of properties that are significant to the user [14]:

Total solid content (TSC) – content of rubber and all non-rubber constituents, determined by evaporation of latex and expressed as a weight percentage of the weight of latex.

Dry rubber content (DRC) – content of rubber and part of the non-rubber constituents determined by precipitation of latex under standardized conditions and expressed as a weight percentage of the weight of latex.

Alkalinity – the alkalinity is expressed as grams of ammonia per 100 g of water in the latex.

Potassium hydroxide (KOH) number – In ammonium-preserved latex, KOH number is defined as the number of grams of potassium hydroxide equivalent to the acids present as ammonium salts in a quantity of latex containing 100 g of solids.

The KOH number has a twofold significance. First, it is regarded as a general index of quality. The higher the number, the poorer being the quality of the latex. Micro-organic activity tends to produce acids which, in the presence of ammonia, form ammonium salts. Second, the KOH number gives the minimum quantity of potassium

hydroxide which must be added to the latex in order to ensure the virtual absence of ammonium ions.

Volatile fatty acids (VFA) number – Volatile fatty acids measured in the VFA test consist primarily of acetic and formic acids. These are present as a result of bacteria activity in the latex. The VFA number of a latex is defined formally as the number of grams of potassium hydroxide equivalent to the steam-volatile fatty acids which are produced by the acidification of latex containing 100 g of solids. The VFA number also provides a good guide to latex quality.

Latex mechanical stability time (MST) – The mechanical stability time of a latex is one of the most important measures of latex stability and indicates the resistance of the latex to aggregation destabilization by shear forces. Shear forces are encountered in operation such as pumping, transportation, compounding and processing of the latex.

The general procedure for mechanical stability determination is to stir a defined amount of latex under given conditions of dilution, temperature and speed of stirring, then measure the time which elapses before signs of incipient agglomeration appear. The mechanical stability is expressed in seconds.

Sludge content – sludge refers to non-polymer impurities which tend to sediment under the influence of gravity. They are dirt, sand, bark fragments and magnesium ammonium phosphate.

The rubber solids content and the alkalinity are considered relatively fixed properties, if properly stored, these properties should remain largely unchanged. In contrast, properties such as KOH number, VFA number and MST are, time dependent and also depend on the effectiveness of preservation, handling procedures and storage.

1.3.3 Latex types

In principle, Hevea latex has been classified according to the methods used for their concentration and stabilization. The current types of latex and their preservative systems are shown in table 1.1.

Table 1.1 Commercial types of latex concentrate [15].

	Preservation system	Designation
Centrifuged	High ammonia	HA
	Low ammonia-TMTD/zinc oxide	LA-TZ
	Low ammonia-sodium pentachlorophenate	LA-SPP
	Low ammonia-boric acid	LA-BA
	Low ammonia-zinc diethyl dithiocarbamate	LA-ZDC
Creamed	High and low ammonia types	As above
Evaporated	Potassium hydroxide (68-73% TSC)	-
	Ammonia (62%TSC)	-
Prevulcanized	High ammonia and low ammonia	-
MG grafted (latex grafted with methyl methacrylate)	High ammonia	MG
Hydroxylamine treated	High ammonia	HRH
Multicentrifuged	High ammonia	HA-DC

High ammonia (HA) latex, containing 0.7% ammonia in the latex, is still the most frequently used material. More than 60 percent of centrifuged latex is of the high ammonia type. However, in recent years, the trend has been toward the use of low ammonia (LA) lattices, in particular the LA-TZ (low ammonia-tetramethythiuram

disulfide,TMTD/zinc oxide) which ensure good color and chemical stability of the films and a low toxicity of the latex. The two-component system serves as a secondary stabilizing agent, in which one component-zinc oxide acts as an enzymic poison and the other component-TMTD has bactericidal properties. The low ammonia latex contains 0.2% of ammonia, with the addition of either 0.2% of sodium pentachlorophenolate (LA-SPP latex), 0.2% of boric acid (LA-BA latex) or 0.1% of zinc diethyldithiocarbamate (LA-ZDC latex). The use of LA latex should reduce ammonia in the factory environment and also eliminate the deammoniation step required in some processing, resulting in cost-saving. These merits are now increasingly being recognized.

1.4 Nanocomposites

Layered silicates dispersed as a reinforcing phase in an engineering polymer matrix are emerging as a relatively new form of useful materials. These composites exhibit a change in composition and structure over a nanometer length scale and posses remarkable property enhancements relative to pure polymer. Owing to the nanometer-size particles obtained by dispersion, these nanocomposites exhibit superior properties such as mechanical, thermal, optical and physico-chemical properties at a lower level loading compared with either the pure polymer or conventional micron sized composites. Their unique properties stem from a combination of factors: the platelet structure of nanolayer clay, the high aspect ratio (width to thickness) of the platelets with thicknesses on the order of a nanometer and widths and lengths on the order of 500-2000, and the molecular bonds formed between the platelets and the polymer during compounding that may modify polymer properties.

It has been demonstrated that the complete dispersion of clay nanolayers in a polymer optimizes the number of available reinforcing elements carrying an applied load and deflecting cracks [16]. Coupling between the tremendous surface area of the clay in the platelet form (750 m^2/g) and polymer molecules that constitute the matrix, facilitates stress transfer to the reinforcement phase, allowing for improvements in tensile and toughness properties. Conventional polymer-clay composites containing aggregated nanolayer tactoids (micron sized particles) ordinarily improve rigidity, but they often sacrifice strength, elongation and toughness. The high aspect ratio characteristic of silicate nanolayers in exfoliated nanocomposites has also been found to greatly reduce gas and water permeability by imposing a tortuous pathway that a permeant has to travel in order to bypass impermeable clay layers [17-18]. Enhanced barrier characteristics, chemical resistance, reduced solvent uptake and flame retardance of clay-polymer nanocomposites all benefit from the hindered diffusion pathway through the nanocomposite.

1.4.1 Structure of layered silicates

Clay minerals are hydrous aluminum silicates and are classified as phyllosilicates, or layer silicates. The silicates commonly used in nanocomposites belong to the structural family of 2:1 phyllosilicates. All layer silicates can be imagined as constructed from two modular units [19]: A sheet of corner-linked tetrahedra and a sheet of edge-shared octahedra. The 2:1 type layer structure is made up of two tetrahedral sheets of silica fused to an octahedral sheet of either aluminum (gibbsite) or magnesium (brucite) hydroxide as illustrated in figure 1.1. The layer thickness is approximately 1 nm and the

lateral dimension of these layers may vary from 300 Å to several microns and even larger depending on the particular silicate. These layers organize themselves to form stacks with a regular electrostatic and van der Waals bonded gap between them called the interlayer or gallery.

Various layer silicates are classified as dioctahedral or trioctahedral. In clay minerals, the smallest structural unit contains three octahedral sites. If all three octahedral sites are occupied, i.e. have octahedral cations at their centers, the sheet is classified as trioctahedral. If only two octahedral sites are occupied and the third octahedron is vacant, the sheet is classified as dioctahedral. The 2:1 type layer silicates have various cation substitutions in both the tetrahedral and octahedral positions. Substitutions within the layers by ions of lesser charge, notably Si^{4+} by Al^{3+} in tetrahedral positions and Al^{3+} or Fe^{3+} by Mg^{2+} or Fe^{2+} in octahedral positions, result in negative charges on the layers. These are normally counterbalanced by alkali or alkali earth cations situated in the interlayer space. In pristine layer silicates the interlayer cations are usually hydrated Na^{+}, K^{+}, Ca^{2+} and Mg^{2+} ions but a wide range of other cations, including organic ions, can be introduced by exchange reactions [21].

The replacement of inorganic exchange cations in the galleries of the native clay by cationic surfactants such as alkylammonium ions is known to help compatibilize the surface chemistry of the clay and the hydrophobic polymer matrix. The role of alkylammonium cations in the organosilicate is to lower the surface energy of the inorganic host and improve its wetting characteristics with the polymer. Additionally, organic cations may provide various functional groups that can react with the polymer to

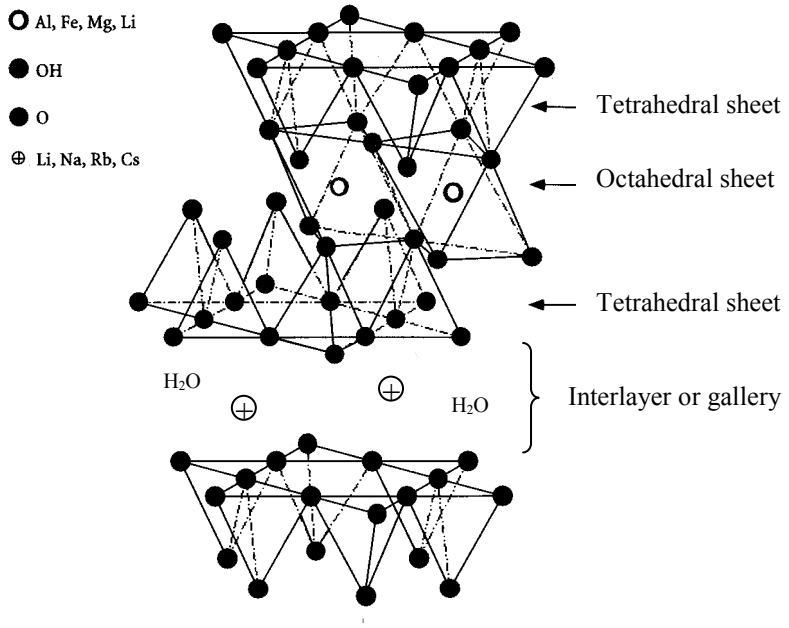

Figure 1.1 Structure of 2:1 phyllosilicates [20].

Table 1.2 Chemical structure of commonly used 2:1 layered silicates [10,20].

2:1 phyllosilicate	General formula
Montmorillonite	$M_x[Al_{4-x}Mg_x](Si_8)O_{20}(OH)_4$
Hectorite	$M_x[Mg_{6-x}Li_x](Si_8)O_{20}(OH)_4$
Saponite	$M_x[Mg_6]\ (Si_{8-x}Al_x)O_{20}(OH)_4$

M = monovalent charge compensating cation in the interlayer
x = degree of isomorphous substitution (between 0.5-1.3)

improve adhesion or initiate polymerization of monomers to improve the strength of the interfacial bond between the silicate and the polymer [22].

Montmorillonite, hectorite and saponite are the most commonly used layer silicates. Their chemical formulas are shown in table 1.2. These clay minerals are characterized by a moderate negative surface charge (cation exchange capacity, CEC), a large active surface area (700-800 m^2/g in the case of montmorillonite) and a plate-like morphology. Their layer charge varies from layer to layer and must be considered as an average value over the whole crystal. Only a small part of the charge balancing cations are located on the external crystallite surface, the majority of these exchangeable cations is located in the interlayer space. In the pristine layer silicate, when hydrated metal cations from the interlayer are ion-exchanged with organic cations such as an alkylammonium or an alkylphosphonium, the layer silicate attains a hydrophobic/ organophillic character and typically results in a larger interlayer spacing.

1.4.2 Nanocomposite Structure

Three main types of composites may be obtained when a layered clay is associated with a polymer [10,23]. These primarily depend on the method of preparation and the nature of components used (layered silicates, organic cation and polymer matrix).

When the polymer is unable to intercalate between the silicate layers, a **phase separated** polymer/ silicate composite is obtained (Fig. 1.2a). This conventional composite contains clay tactoids of stacked layers in a coplanar orientation, that are associated in aggregates and agglomerates dispersed as a segregated phase. Their properties stay in the same range as those seen for traditional microcomposites. Beyond

this classical family of composites, two types of nanocomposites are possible. **Intercalated** structures in which typically more extended polymer chains are pictured as occupying the interlayer space between silicate layers resulting in a well ordered multilayer morphology of alternating polymeric and inorganic layers (Fig. 1.2b). When the silicate layers (1 nm thick) are completely and uniformly dispersed in a continuous polymer matrix, an **exfoliated** or **delaminated** structure is obtained (Fig. 1.2c).

The structure of polymer layered silicate (PLS) nanocomposites has traditionally been elucidated using x-ray diffraction (XRD) and transmission electron microscopy (TEM). XRD is the most commonly used technique to identify intercalated structures due to the periodic arrangement of the silicate layers both in the pristine and the intercalated states. The repetitive multilayer structure is well preserved in intercalated structures, allowing the interlayer spacing to be determined. Intercalation of polymer chains usually increases the interlayer spacing, in comparison to the spacing of the original silicate, resulting in a shift of the X-ray diffraction (XRD) peak toward lower angles. The diffraction angle is related to the layer spacing through the well known Bragg's relation $\lambda = 2d\sin\theta$.

In the case of exfoliated structures, extensive layer separation associated with delamination of the original silicate structure in the polymer matrix leads to the disappearance of any coherent x-ray scattering from the layers. Loss of coherent scattering may be due to either the presence of an extremely large regular ordered spacing between the layers, too large to be detected in the angular range of XRD normally operated, or the nanocomposite no longer has an ordered layer structure. TEM is therefore used to determine nanocomposite morphology. In addition to these two defined

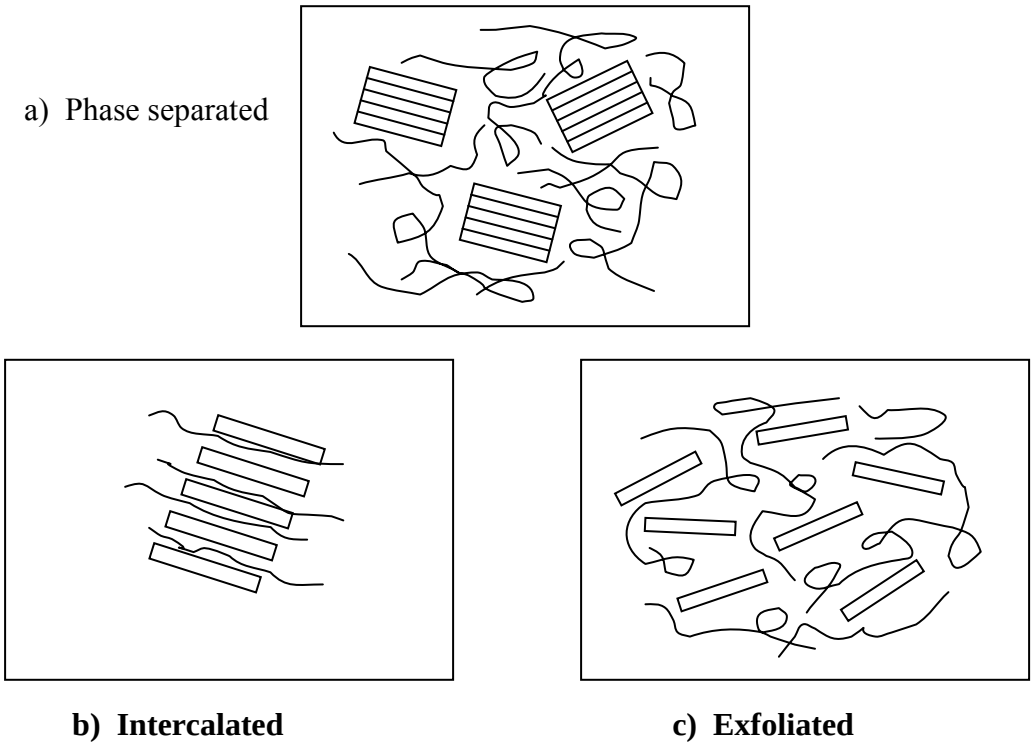

Figure 1.2 Schematic representation of different polymer/silicate hybrid structures.

structures, both intercalation and partial exfoliation result in a broadening of the diffraction peak.

1.5 Mechanical Properties

Layered silicates are potentially well-suited for use as reinforcing materials. They have chemically stable siloxane surfaces and a high surface area. They also posses high in-plane strength, stiffness, and a high aspect ratio. Moreover, the rich intercalation chemistry of clay silicate can be used to facilitate exfoliation of silicate nanolayers into the polymer network. Layer exfoliation maximizes interfacial contact between the organic and inorganic phases. Tensile properties have been proved to be greatly enhanced by the reinforcing effect of silicate nanolayers.

1.5.1 Effect on tensile modulus

The tensile modulus (or Young's modulus), expressing the stiffness of a material in the initial deformation stage of sample undergoing a tensile test, has been shown to be tremendously improved when nanocomposites are formed.

The advantage of hybrids containing single silicate layers uniformly dispersed in a polymer matrix were first demonstrated by researchers at Toyota in Japan for **nylon-6** nanocomposite [24-26]. Their nylon-6 obtained through the intercalative ring opening polymerization of ε-caprolactam, leading to the formation of exfoliated nanocomposites show a dramatic increase in Young's modulus at low filler content. Incorporation of only 5 wt% clay resulted in approximately 70% increase in Young's modulus and 40% increase in tensile strength. Flexural modulus and strength increased by 126% and 60% respectively. Interestingly, the substantial increases in strength and modulus were not

accompanied by a decrease in impact resistance as is usually the case with filled polymers. When using conventional micron sized mineral fillers, loadings as high as 30% were needed to achieve the same gains in modulus with a loss in impact strength.

In addition, exfoliated nanocomposites from montmorillonite (with average platelet length of 1000 angstroms) show values of Young's modulus superior to nanocomposites from saponite (average length: 500 angstroms) as illustrated in Figure 1.3. This clearly indicated that the ability of dispersed silicate layers to increase the tensile modulus of nylon-6 nanocomposite can be directly related to the average length of the platelets, hence to the aspect ratio of dispersed nanoparticles.

Moreover, differences in the extent of exfoliation was also seen to strongly influence the measured Young's modulus [27]. Table 1.3 shows the XRD peak intensity (I_m) and Young's modulus of various nylon-6 based nanocomposites synthesized by a one-step in situ intercalative polymerization of ε-caprolactam using Na-montmorillonite in the presence of different acids. Depending on the acid added to catalyze the polymerization, one can observe variation of the XRD peak intensity (I_m) which is inversely related to the amount of exfoliated layers in the nanocomposite. An increase in tensile modulus is observed with a decrease in I_m values. The excellent mechanical properties of nylon-6 clay hybrid systems were considered to have their origin in the dispersed silicate layer and the degree of dispersion.

Clay nanolayers have also been shown to be very effective reinforcement in **epoxy** systems. The key to achieve an exfoliated epoxy-clay nanocomposite structure is first to load the clay gallery with hydrophobic onium ions, and then expand the gallery region by diffusing in the epoxide and the curing agent. Dramatic improvement in

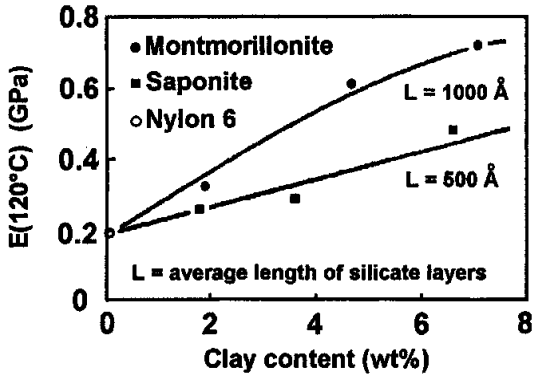

Figure 1.3 Dependence of tensile modulus at 120°C on clay content for organo-modified montmorillonite and saponite based nanocomposites [24].

Table 1.3 Peak intensity (I_m) and Young's modulus of various nylon-6 based nanocomposites in the presence of different acids [27].

Acid	I_m (cps)	Young's modulus (GPa)
Phosphoric acid	0	2.25
Hydrochloric acid	200	2.05
Isophthalic acid	255	1.74
Benzenesulfonic acid	280	1.74
Acetic acid	555	1.63
Trichloroacetic acid	585	1.67

modulus as well as tensile strength was realized, particularly when the matrix exhibited a subambient glass transition temperature. For instance, incorporation of 15 wt% (7.5 vol%) of the exfoliated organoclay improves the strength of an elastomeric epoxy polymer matrix more than 10-fold [28]. Reinforcing performance of epoxy-clay hybrids was also shown to depend on the chain length of the alkylammonium cation which greatly affected the extent of clay expansion upon epoxide intercalation. At a loading of 10 wt% $CH_3 (CH_2)_{n-1}NH_3^+$ - montmorillonite, the mechanical properties increased with increasing clay exfoliation in the order $CH_3 (CH_2)_7NH_3^+$- < $CH_3 (CH_2)_{11} NH_3^+$ - < $CH_3 (CH_2)_{17} NH_3^+$- montmorillonite. It was concluded that exfoliated clay composites are favored over intercalated analogues for improving the mechanical performance of the polymer.

Exfoliation of layered materials such as magadiite in an ***elastomeric epoxy*** matrix also gives rise to a remarkable increase in Young's modulus of the composites [29] as denoted in Figure 1.4. This figure compares the modulus for epoxy-magadiite and epoxy-montmorillonite exfoliated nanocomposites with filler loading. The montmorillonite based nanocomposites show a significant increase in tensile modulus at high silicate loading (>4wt%). These difference in reinforcement properties were attributable to the difference in the layer charge density between organomagadiite and montmorillonite. Organomagadiites have a higher layer charge density, and therefore a higher alkylammonium ion content than organomontmorillonite. Since the alkylammonium ions interact with the epoxy resin during polymerization, dangling polymer chains are formed. These dangling chains are known to weaken the polymer

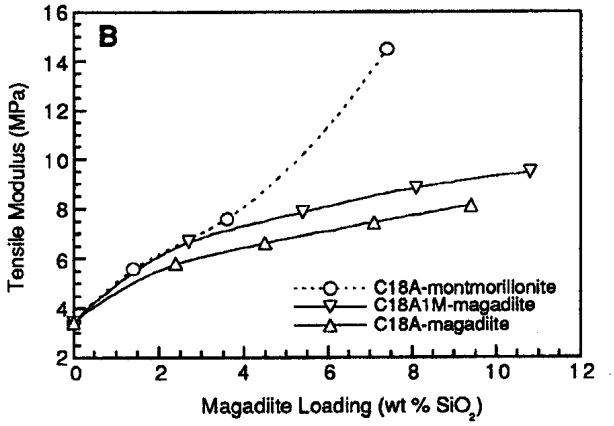

Figure 1.4 A comparison of tensile moduli for epoxy nanocomposites prepared from various organo modified fillers: C18A- montmorillonite = montmorillonite modified with octadecylammonium, C18A- and C18A1M- magadiite = magadiite modified with octadecylammonium and methyl–octadecylammonium respectively [29].

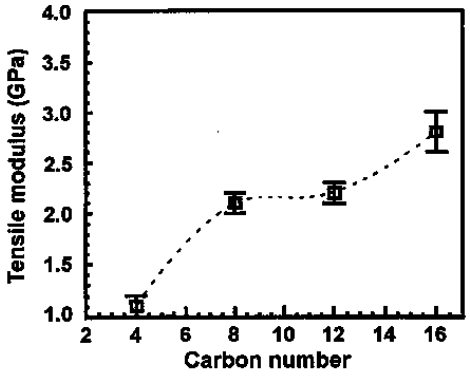

Figure 1.5 Dependence of tensile modulus of amine-cured epoxy–clay nanocomposites on onium ion carbon number at clay loading of 2 wt% [30].

matrix by reducing the degree of network crosslinking which compromises the reinforcement effect of silicate layer exfoliation.

A large increase in the tensile modulus for an exfoliated structure is also observed for ***thermoset epoxy*** matrices [30-31]. Figure 1.5 illustrates the modulus for various amine-cured epoxy nanocomposites filled with 2wt% montmorillonite modified by alkylammonium cations of different length. Montmorillonite modified with butylammonium formed an intercalated structure exhibiting a low tensile modulus, while the other three nanocomposites with alkyl chains of 8, 12 and 16 carbons are characterized by exfoliated structures as determined by TEM and XRD, and give much higher modulus values.

In contrast, exfoliation was not reported to be a prerequisite to improve the stiffness of elastomeric **polyurethane** matrices, whose performance was greatly improved in a cross-linked soft polyurethane nanocomposite [32]. At a loading of only 10 wt% organoclay the modulus, strength and strain at break all were increased by more than 100%, a plot of modulus is shown in figure 1.6. Apparently clay nanolayers, even when aggregated in the form of intercalated tactoids, stiffen, strengthen and toughen the matrix.

Modulus improvement was also demonstrated in a **polypropylene** nanocomposite obtained by melt intercalation with organophilic clay using maleic anhydride-modified PP oligomer (PP-MA) as a compatibilizer [33]. The modulus of a PP-clay hybrid with 5 wt% clay and 22 wt% PP-MA was 1.8 times higher than that of PP at 80°C. It was also shown that increasing the amount of PP-MA not only improved intercalation and partial exfoliation, but also increased the tensile modulus.

In nanocomposites having an intercalated structure (without any apparent exfoliation), such as **PMMA** (polymethylmetacrylate) [34] and **PS** (polystyrene) [35], the increase in Young's modulus is relatively weak. PS-clay hybrids obtained by emulsion polymerization using water-swollen Na-montmorillonite show a modulus increase from 1.21 to 1.30 GPa for pure PS, and PS containing 11.3 wt% montmorillonite, respectively. This suggests that intercalated structures are inefficient in improving the stiffness of nanocomposites.

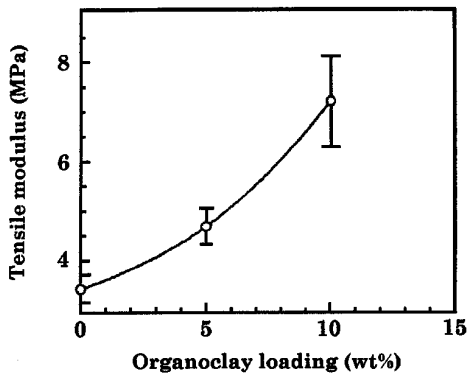

Figure 1.6 Tensile modulus VS. organoclay loading for elastomeric polyurethane-clay nanocomposite [32].

1.5.2 Stress at break

Stress at break, the ultimate strength that the material can bear before it breaks, varies strongly depending on the nature of interactions between the matrix and the filler. Table 1.4 summarize tensile stress of various thermoplastic-based nanocomposites.

One can see from the table that an increase in the stress at break is obvious in filled polymers such as exfoliated **nylon-6** [24] and intercalated **PMMA** [34] nanocomposites. This has been explained by the presence of ionic interactions of nylon grafted to the silicate layer, and the presence of polar PMMA. This increase is much more pronounced in the case of nylon-6 which has both an exfoliated structure and ionic bonds with the silicate layers. In **polypropylene** [33] nanocomposites, tensile strengths were almost equivalent to that of the PP matrix. This behavior was explained by the lack of interfacial adhesion between apolar PP and polar layered silicates. However, addition of maleic anhydride modified- PP to the PP matrix has proved to be favorable to the intercalation of PP chains and maintains the strength at an acceptable level. The ultimate tensile stress in **PS**-intercalated nanocomposite [35] show a large decrease and further decreases at higher filler content. This was mainly ascribed to the weak interactions between PS matrix and clay particles.

Epoxy [28-31] resin based nanocomposites display a different behavior depending upon their glass transition temperature, either above or below room temperature. For the case of high T_g epoxy thermoset, neither intercalated nor exfoliated nanosilicates lead to and improvement of tensile strength and modulus. In contrast, elastomeric epoxy nanocomposite exhibit a noticeable increase in tensile stress at break as well as previous observed in Young's modulus. Owing to the increased elasticity of

Table 1.4 Tensile stress of nanocomposites [10].

Matrix	Nanofiller content (wt%)	Nanocomposite type	Matrix tensile stress (MPa)	Nanocomposite tensile stress(MPa)	Reference
Nylon-6	4.7	NCH[a]	68.6	97.2	[24]
	4.1	One pot- NCH[b]	68.6	102	[27]
PMMA	12.6	Intercalated	53.9	62.0	[34]
	20.7	Intercalated	53.9	62.0	[34]
PP	5.0	Intercalated[c]	31.4	29.5	[33]
	4.8	Intercalated[d] (exfoliated)	32.6	31.7	[33]
PS	11.3	Intercalated	28.7	21.7	[35]
	17.2	Intercalated	28.7	23.4	[35]
	24.6	Intercalated	28.7	16.6	[35]
	34.1	Intercalated	28.7	16.0	[35]

[a]NCH (Nylon 6-clay hybrid): exfoliated NCH synthesized by in situ intercalated polymerization of ε-caprolactam in 12-aminolaulic acid modified montmorillonite.

[b]One-pot NCH : exfoliated NCH prepared by in situ intercalated polymerization of ε-caprolactam by phosphoric acid in Na-montmorillonite.

[c]PP melt blended with clay intercalated PP-MA of composition 1/1 by weight clay:PP-MA.

[d]PP melt blended with clay intercalated PP-MA of composition 1/3 by weight clay:PP-MA.

the matrix above T_g, the improvement in reinforcement was due to shear deformation and stress transfer to the platelet particles. In addition, platelet alignment under strain may also contribute to the improved performance of clays exfoliated in a rubbery matrix as compared to a glassy matrix. Figure 1.7 proposes a model [28] for the fracture of a glassy and a rubbery matrix. Propagation of fracture across the polymer matrix containing aligned silicate layers is energy consuming, and the tensile strength and modulus are reinforced. In a glassy matrix, clay particle alignment upon applied strain is minimal and blocking of crack growth by exfoliated clay is less efficient.

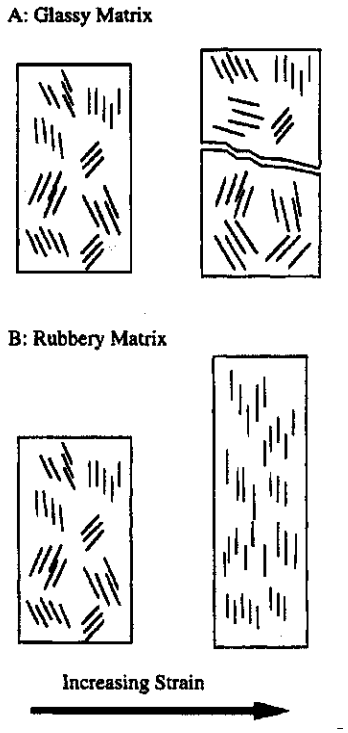

Figure 1.7 Proposed model for the fracture of (A) a glassy and (B) a rubbery polymer clay exfoliated nanocomposite with increasing strain [28].

1.5.3 Elongation to break

The elongation at break of nanocomposites has not been widely investigated. In thermoplastics such as intercalated **PMMA** [34], the elongation at break decreased with increasing clay content. The same behavior was also observed in **PS** nanocomposites prepared by emulsion polymerization [35]. A considerable loss in ultimate elongation was observed in intercalated-exfoliated **PP** [33] which exhibited brittle fracture. The elongation at break dropped from 150% for pure PP matrix to 105% for a 6.9 wt% clay microcomposite, and down to 7.5% for a PP nanocomposite filled with 5 wt% silicate layers.

Elastomeric **epoxy** [29] and **polyurethane** [32] nanocomposites did not show a loss in ultimate strain. Polyurethane matrices exhibited a two-fold increase in elongation at break, as well as in modulus and strength as discussed earlier, with only 10 wt% organoclay. These tensile properties all increase with increasing loading of silicate nanolayers. The improved elasticity was attributed in part to the plasticizing effect of gallery onium ions, which contribute to dangling chain formation in the matrix, as well as to conformational effects on the polymer at the clay-matrix interface.

Another hybrid which exhibits both an increase in tensile strength and elongation at break is **polyimide** [36] filled with montmorillonite exchanged with hexadecylamine. These improvements increased with clay content up to 5 wt%. At higher filler loading, both properties experienced a sharp drop towards values lower than those of the matrix alone. This decrease was explained by aggregation of montmorillonite at higher loadings, which causes the composites to be much more brittle.

REFERENCES

1. Morton, M., Editor (1987) Rubber Technology, 3 ed., Van Nostrand Reinhold Co., New York, 631 pp.
2. Blackley, D. C. (1966) High Polymer Lattices; Their Science and Technology: Volume 1 Fundamental Principles, Palmerton Publishing Co., New york, 351 pp.
3. Winspear, G. G., Ed. (1954) The Vanderbilt Latex Handbook, R.T. Vanderbilt,
4. Rothon, R., Editor (1995) Particulate-Filled Polymer Composites, Longman Scientific & Technical, New York, 371 pp.
5. Blow, C. M., Editor (1971) Rubber Technology and Manufacture, The Chemical Rubber Co., Ohio, 509 pp.
6. Dick, J. S., Editor (2001) Rubber Technology: Compounding and Testing for Performance, Hanser Publishers, 523 pp.
7. Eirich, F. R., Editor (1978) Science and Technology of Rubber, Academic Press, New York, 633 pp.
8. Franta, I., Editor (1989) Elastomers and Rubber Compounding Materials, Elsevier, New York, 588 pp.
9. Burnside, S. D. and Giannelis, E. P. (1995) Synthesis and Properties of New Poly(dimethylsiloxane) Nanocomposites, Chem. Mater.,7(9), 1597-1600.
10. Alexandre, M. and Dubois, P. (2000) Polymer-layered Silicate Nanocomposites: Preparation, Properties and Uses of a New Class of Materials, Mater. Sci. Eng.,28, 1-63.
11. Theng, B. K. G. (1979) Formation and Properties of Clay-Polymer Complexes, Elsevier Scientific Publishing Company, New York, 353 pp.

12. Robert, A. D., Editor (1988) Natural Rubber Science and Technology, Oxford Science Publications, 1078 pp.
13. Odian, G. (1991) Principles of Polymerization, John Wiley & Sons, 749 pp.
14. Blackley, D. C. (1966) High Polymer Lattices; Their Science and Technology: Volume 2 Testing and Applications, Palmerton Publishing Co., New york, 843 pp.
15. Poh, W. N. (1989) Development in Natural Rubber Latex: Production, Properties, Stability, Elastomerics, 121, 9-15.
16. LeBaron, P. C. et al (1999) Polymer-Layered Silicate Nanocomposites: An Overview, Applied Clay Science,15, 11-29.
17. Messersmith, P. B. and Giannelis. E. P. (1995) Synthesis and Barrier Properties of Poly (ε-Caprolactone)-Layered Silicate Nanocomposites, J. of poly Sci-Part A: Polymer Chemistry, 33, 1047-1057.
18. Yano, K. et al (1993) Synthesis and Properties of Polyimide-Clay Hybrid, J. of poly Sci-Part A: Polymer Chemistry, 31, 2493-2498.
19. Moore, D. M. and Reynolds, R. C. Jr. (1997) X-ray Diffraction and the Identification and Analysis of Clay Minerals, Oxford, New York, 378 pp.
20. Giannelis, E. P. et al (1999) Polymer-Silicate Nanocomposites: Model Systems for Confined Polymers and Polymer Brushes, Adv. Polym. Sci, 138, 107-143.
21. Newman, A. C. D. (1987) Chemistry of Clays and Clay Minerals, Wiley, New York, 480 pp.
22. Krishnamoorti, R., et al (1996) Structure and Dynamics of Polymer-Layered Silicate Nanocomposite, Chem. Mater. 8, 1728-1734.

23. Giannelis, E. P. (1996) Polymer Layered Silicate Nanocomposites, Adv. Mater., 8(1), 29-35.

24. Kojima, Y. et al (1993) Mechanical Properties of Nylon 6-clay Hybrid, J. Mater. Res., 8 (5), 1185-1189.

25. Usuki, A. et al (1993) Synthesis of Nylon 6-Clay Hybrid, J. Mater. Res., 8 (5), 1179-1184.

26. Usuki, A. et al (1993) Swelling Behavior of Montmorillonite Cation Exchanged for ω-Amino Acids by ε-Caprolactam, J. Mater. Res., 8 (5), 1174-1178.

27. Kojima, Y. et al (1993) One Pot Synthesis of Nylon 6-Clay Hybrid, J. Polym. Sci. Part A: Polymer Chemistry, 31,1755-1758.

28. Wang, Z. and Pinnavaia, T. J. (1998) Hybrid Organic-Inorganic Nanocomposites: Exfoliation of Magadiite Nanolayers in an Elastomeric Epoxy Polymer, Chem. Mater, 10, 1820-1826.

29. Lan, T. and Pinnavaia, T. J. (1994) Clay-Reinforced Epoxy Nanocomposites, Chem. Mater, 6, 2216-2219.

30. Lan, T. and Kaviratna, P. D. (1995) Mechanism of Clay Tactoid Exfoliation in Epoxy-Clay Nanocomposites, Chem. Mater, 7, 2144-2150.

31. Zilg, C., et al (1999) Morphology and Toughness/Stiffness Balance of Nanocomposites Based upon Anhydride-Cured Epoxy Resins and Layered Silicates, Macromol. Chem. Phys., 200, 661-670.

32. Wang, Z. and Pinnavaia, T. J. (1998) Nanolayer Reinforcement of Elastomaric Polyurethane, Chem. Mater, 10, 3769-3771.

33. Hasegawa, N., et al (1998) Preparation and Mechanical Properties of Polypropylene-Clay Hybrids Using a Maleic Anhydride-Modified Polypropylene Oligomer, J. of Appl. Polm. Sci, 67, 87-92.

34. Lee, D. C. and Jang, L. W. (1996) Preparation and Characterization of PMMA-Clay Hybrid Composite by Emulsion Polymerization, J. Appl. Polym. Sci., 61, 1117-1122.

35. Noh, M. W. and Lee, D. C. (1999) Synthesis and Characterization of PS-Clay Nanocomposite by Emulsion Polymerization, Polym. Bull, 42, 619-626.

36. Yang, Y. et al (1999) Preparation and Properties of Hybrids of Organo-Soluble Polyimide and Montmorillonite with Various Chemical Surface Modifications Methods, Polymer, 40, 4407-4414.

CHAPTER 2

THEORY OF REINFORCEMENT

2.1 Scope

This chapter provides a general overview of reinforced composite systems and an understanding of the properties of fillers and filled composites, focusing primarily on clay-filled rubber. Two main principal types of composites are covered, namely particulate-filled and fiber-filled polymers. In addition, a theoretical underpinning for determining composite properties, in particular the elastic modulus, will be presented. Furthermore, the effects of filler concentration (volume fraction), size, shape and agglomeration are examined as well as interfacial interaction between phases. There are several factors that can affect the behavior of filled systems. However, these factors are often difficult to separate and to evaluate in a quantitative manner.

2.2 Introduction to composite systems

Composite materials may be defined as materials having two or more distinct components or phases and their components have significantly different physical properties and thus, the composite properties are noticeably different from the individual component properties. Composites consist of one or more discontinuous phases embedded in a continuous phase. The discontinuous phase is usually harder and stronger than the continuous phase and is called the reinforcement or reinforcing material, whereas the continuous phase is termed the matrix. Composite materials may be classified into two broad groups on the basis of reinforcement geometry [1]:

(1) particulate-filled materials consisting of a continuous matrix phase and a discontinuous filler phase made up of discrete particles which can be spherical, cubic, block and platelet (or flake), and

(2) fiber-filled composites. A fiber is characterized by the fact that its length is much greater than its cross-sectional area.

The properties of composite materials are strongly influenced by the properties of the components, by the geometry of the filler phase (size, shape and size distribution), by the morphology of the system, and by the nature of the interface between the phases [2]. Composite properties may be simply described by the volume fraction sum of the properties of their components or they may provide properties that are not accounted for by this simple relationship. Therefore, all these factors (and perhaps others) are important in determining the composite properties. However, not all factors are accounted for in the development of a theoretical description of composites.

2.3 Composites with flake reinforcement

Thin flakes offer attractive features for an effective reinforcement. They have primarily a two-dimensional geometry and hence impart equal strength in all direction in their plane compared to fibers that offer a unidirectional reinforcement. An important group of planar reinforcements are composites containing minerals such as clay, platy talc, and mica which are widely employed as fillers in polymers [3]. Their incorporation normally imparts higher stiffness and higher resistance to heat distortion, and leads to lower shrinkage and a decrease in the coefficient of thermal expansion. However, the increase in tensile strength is rather limited and ductility is often decreased. In order for flakes to provide full reinforcement potential, platelets are required that have as high an

aspect ratio as possible and a strong adhesion to the matrix. These two conditions are necessary to ensure efficient stress transfer between the two components. In addition, polymers filled with plate-like particles posses an extremely high resistance to the permeation of gases and liquids, which is attributable to flakes or platelets being aligned parallel to the surface of the film or sheet during processing [4].

An understanding of the mechanisms involved in flake reinforcement in composites has been developed from a knowledge of fiber reinforced composites [3, 5-6]. Reinforcement conditions are based on the same general principle of reinforcement that apply to short fibers. It is, therefore, worth examining the theoretical determination of fiber-filled systems.

2.4 Fiber–reinforced composites

Fiber reinforcing structures are often divided into two types, continuous and discontinuous reinforcement. Composites with long fibers are called continuous–fiber reinforced composites, and those with short fibers are discontinuous–fiber reinforced composites. “Long” and ‘short” are often defined in terms of a fiber length (L) to diameter (d) ratio. L/d ratios > 100 are considered to be effectively continuous. Most fiber- filled composites are anisotropic with tremendous strength in the fiber long axis direction which is readily seen when the sample is made with the fiber filler oriented in a particular direction. Such uniaxially oriented materials require at least five or six independent elastic moduli to describe their stiffness character [2], and their properties are different in different directions.

2.4.1 Moduli of Fiber-reinforced Composites

The simplest type of continuous reinforcement is one where fibers are all aligned parallel to each other in a single direction throughout the matrix to form a uniaxial composite. Such a composite has the strongest properties in the longitudinal direction, i.e. along the fiber direction. The five engineering moduli of uniaxially oriented fiber composite are illustrated in figure 1. Those are (1) the longitudinal Young's modulus, E_L, in which the load is applied parallel to the fibers; (2) the transverse Young's modulus, E_T, in which the load is applied perpendicular to the fibers; (3) the longitudinal-transverse shear modulus, G_{LT}, in which shearing stress in the polymer acts in a direction along the fibers; (4) the transverse shear modulus, G_{TT}, in which the shearing stress is applied perpendicular to the fibers; and (5) a bulk modulus K.

2.4.1A <u>The longitudinal modulus</u>

The simple rule of mixtures accurately predicts the stress-strain behavior of a uniaxially oriented composite that is subjected to longitudinal tensile loads [1]. The basic assumption for a uniaxial composite is as follow:

(1) Fibers are uniform in properties and diameter, continuous, and parallel throughout the composite

(2) Perfect bonding exists between the fibers and the matrix

(3) The composite is free of voids

(4) Applied loads are either parallel or perpendicular to the fiber direction

(5) Both fibers and matrix deform as linearly elastic materials

The following relations are needed to determine the longitudinal modulus, E_L of uniaxially oriented fiber composite.

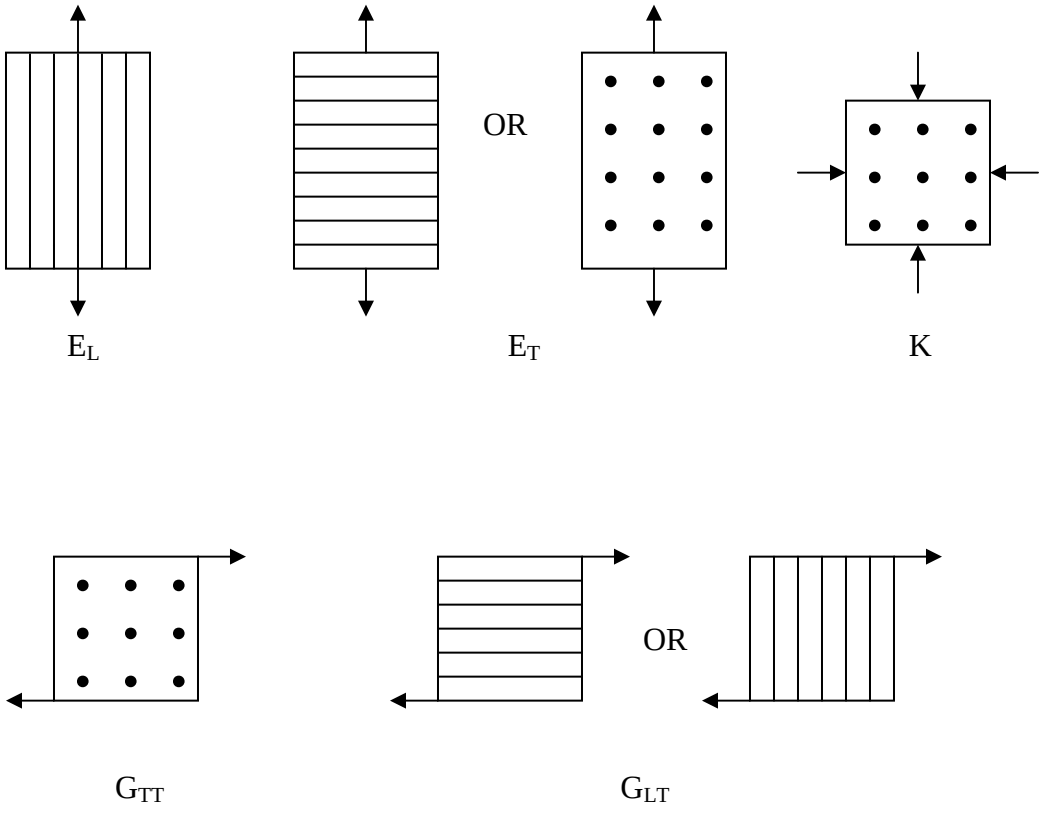

Figure 2.1 The elastic moduli of uniaxially oriented materials [2].

The load (P_c) carried by the composite with parallel continuous fiber is the sum of the loads carried by the fiber (P_f) and the matrix (P_m). In the following equation and throughout, subscripts c, f and m refer to composite, fiber and matrix respectively

$$P_c = P_f + P_m \quad (1)$$

Since there is assumed to be perfect bonding between fiber and matrix, no slippage can occur at the interface and the strain, ε, experienced by fiber, matrix and composite are equal:

$$\varepsilon_f = \varepsilon_m = \varepsilon_c \quad (2)$$

The load P_c can be written in terms of a stress, σ_c acting over the entire cross sectional area, A_c as follows:

$$P_c = \sigma_c A_c = \sigma_f A_f + \sigma_m A_m \quad (3)$$

or

$$\sigma_c = \sigma_f \frac{A_f}{A_c} + \sigma_m \frac{A_m}{A_c} \quad (4)$$

Volume fraction, V for composites with parallel fibers are equal to area fraction, thus

$$V_f = \frac{A_f}{A_c} \quad , \quad V_m = \frac{A_m}{A_c} \quad (5)$$

Therefore $$\sigma_c = \sigma_f V_f + \sigma_m V_m \quad (6)$$

Equation (6) can be differentiated with respect to strain, which is equal for composite, fiber and matrix according to equation (2):

$$\frac{d\sigma_c}{d\varepsilon_c} = \frac{d\sigma_f}{d\varepsilon_f} V_f + \frac{d\sigma_m}{d\varepsilon_m} V_m \quad (7)$$

If the stress – strain curve of the composite material is linear, the slope, dσ/dε, is constant and can be replaced by the elastic modulus, E_c. Thus

$$E_c = E_f V_f + E_m V_m \quad (8)$$

This relationship is known in the composite area as the rule of mixtures. The equation indicates that contributions of fiber and matrix to the average composite properties are proportional to their volume fractions. Such relative proportions of matrix and reinforcing fiber is one of the most important factors in determining the properties of composite materials.

2.4.1B Volume and weight fraction

The relative proportion of the matrix and reinforcing component in composite can be given as the weight fractions or the volume fractions. Weight fractions are more easily obtained experimentally, whereas the volume fractions are exclusively used in a theoretical analysis of composite materials. Thus it is desirable to utilize an expression for conversion between weight fraction and volume fraction.

Consider a composite of volume v_c, consisting of a volume of fibers, v_f and matrix volume, v_m. Let w_c, w_f, and w_m represent the corresponding weight of composite material, fiber, and the matrix respectively. Then the volume fractions (V_f and V_m) and weight fractions(W_f and W_m) are defined as follow [1].

$$v_c = v_f + v_m \quad (9)$$

$$V_f = \frac{v_f}{v_c}, \quad V_m = \frac{v_m}{v_c} \quad (10)$$

and

$$w_c = w_f + w_m \quad (11)$$

$$W_f = \frac{w_f}{w_c}, \quad W_m = \frac{w_m}{w_c} \quad (12)$$

The density of the composite, ρ_c can be obtained in terms of volume fraction of components by replacing equation (11) with

$$\rho_c v_c = \rho_f v_f + \rho_m v_m \quad (13)$$

Dividing both sides of equation (13) by v_c and substituting the definition for volume fractions from equation (10) gives

$$\rho_c = \rho_f \frac{V_f}{V_c} + \rho_m \frac{V_m}{V_c} \quad (14)$$

$$\rho_c = \rho_f V_f + \rho_m V_m \quad (15)$$

Similarly, equation (9) can also be manipulated to obtain the density of composite in terms of the weight fractions:

$$\rho_c = \frac{1}{(W_f/\rho_f) + (W_m/\rho_m)} \quad (16)$$

The conversion between the weight fraction and volume fraction can be obtained by replacing the weight in equation (12) by the products of density and volume as follows

$$W_f = \frac{w_f}{w_c} = \frac{\rho_f v_f}{\rho_c v_c} = \frac{\rho_f}{\rho_c} V_f \quad (17)$$

$$W_f = \frac{\rho_f}{\rho_c} V_f$$

and

$$W_m = \frac{\rho_m}{\rho_c} V_m \quad (18)$$

Volume fraction of filler and matrix can also be written as

$$V_f = \frac{\rho_c}{\rho_f} W_f$$

$$V_m = \frac{\rho_c}{\rho_m} W_m \quad (19)$$

2.4.1C <u>The Halpin-Tsai equation</u>

The rule of mixture as shown in equation (8) holds only for the longitudinal Young's modulus, M_L in the case of continuous long fibers. Oriented short fibers give

smaller moduli in a polymer matrix. Halpin [7] demonstrated the dependence of longitudinal modulus on aspect ratio for oriented short-fiber composites. In addition, a theoretical estimation of stiffness properties employing Halpin-Tsai equations was shown to be in good accord with experimental results.

Halpin and Tsai [8-10] developed a simple and generalized equation for the relative elastic moduli of composite materials which has been modified by Nielsen [11] to take into account the maximum volumetric packing fraction of the filler, P_f. It is suggested that the packing of the filler phase should also be considered in the theory of the moduli of composite systems to give

$$\frac{M_c}{M_m} = \frac{1 + ABV_f}{1 - B\psi V_f} \qquad (20)$$

M_c and M_m are the elastic moduli (shear, Young's, or bulk) of the composite and matrix, respectively.

V_f is the volume fraction of filler phase

The constant, A takes into account such factors as geometry of the filler phase and Poisson's ratio of the matrix

The constant, B takes into account the relative moduli of the filler and matrix phases; Its value is 1.0 for very large M_f / M_m ratios. The quantity B is defined as

$$B = \frac{(M_f/M_m) - 1}{(M_f/M_m) + A} \qquad (21)$$

The factor, ψ depends on the maximum packing fraction, P_f of the filler

$$\psi = 1 + \frac{1 - P_f}{P_f^2} V_f \qquad (22)$$

2.4.1D Halpin-Tsai equation for transverse modulus

Prediction of transverse composite modulus is another Halpin-Tsai equation also modified by Nielsen to include a filler packing factor. The transverse Young's modulus, M_T is approximated by

$$\frac{M_T}{M_m} = \frac{1 + ABV_f}{1 - B\psi V_f} \tag{23}$$

where $A = 0.5$ $B = \frac{(M_f/M_m) - 1}{(M_f/M_m) + A}$ (24)

and $\psi = 1 + \frac{1 - P_f}{P_f^2} V_f$ (25)

The factor ψ takes into account the maximum packing fraction P_f of the fibers. In general, for random close packing, this value is set at $P_f = 0.82$ which lies halfway between cubic packing of fiber, $P_f = 0.785$ and hexagonal packing, $P_f = 0.907$ [11].

The longitudinal – transverse shear modulus G_{LT} can be estimated from [7]:

$$\frac{G_{LT}}{G_m} = \frac{1 + ABV_f}{1 - B\psi V_f} \tag{26}$$

where A = 1.0, and B and ψ are given by the same expression as (24) and (25) and replacing M_f / M_m of equation (24) by G_f / G_m, the shear modulus ratio of the two phases.

The transverse shear modulus G_{TT} can be estimated from

$$\frac{G_{TT}}{G_m} = \frac{1 + ABV_f}{1 - B\psi V_f} \tag{27}$$

where A = 0.5, and B and ψ are defined by the same expression as (24) and (25) with M_f / M_m replaced by G_f / G_m.

A uniaxially oriented fiber composite has its highest modulus in the longitudinal direction. It has been clearly demonstrated that fibers are much less effective in raising

the composite modulus in the transverse direction than in the longitudinal direction. The transverse Young's modulus, M_T is low for aligned fiber composite [12,13].

In the case when the test direction is rotated at angle θ from the fiber direction, there is a tremendous change in modulus. The equation for predicting Young's modulus E_θ at some angle θ to the primary fiber axis direction is given by

$$\frac{1}{E_\theta} = \frac{\cos^4\theta}{E_L} + \frac{\sin^4\theta}{E_T} + \left(\frac{1}{G_{LT}} - \frac{2\nu_{LT}}{E_L}\right)\sin^2\theta\cos^2\theta \quad (28)$$

where ν_{LT} is the Poisson's ratio of the composite for a tensile load applied parallel to the fibers.

2.4.2 Modulus of short- fiber composites

The Halpin-Tsai equations for predicting the transverse modulus of uniaxially oriented fiber composites as discussed above are also useful in predicting the longitudinal and transverse moduli of aligned short-fiber composites. A model of short-fiber or discontinuous fiber composites is shown schematically in figure 2.2.

The stiffness properties can be estimated by employing the Halpin-Tsai equation as follows [7]:

(a) Stiffness estimated in the fiber direction

$$\frac{M_L}{M_m} = \frac{1 + ABV_f}{1 - B\psi V_f} \quad (29)$$

where A = 2 l/d; l/d being an aspect ratio of the fiber

B and ψ are defined by the same expressions as in equations (21) and (22)

(b) The in-plane shear modulus is estimated as

$$\frac{G_{LT}}{G_m} = \frac{1 + ABV_f}{1 - B\psi V_f} \quad (30)$$

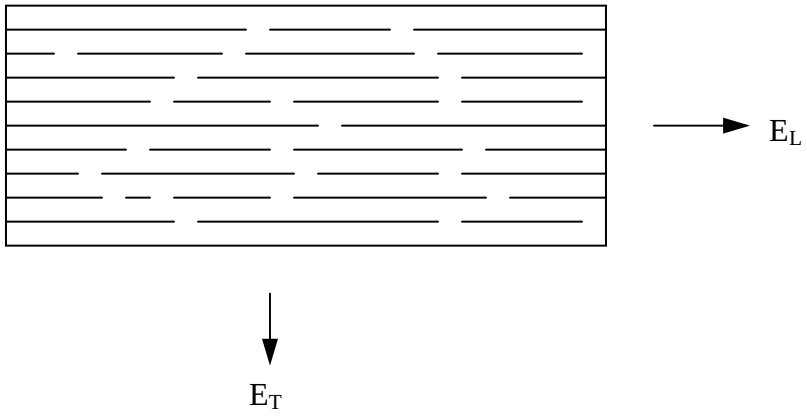

Figure 2.2 Model of aligned short fiber composites [1].

where A = 1.0

B is given by the same expression as (24) except replace M_f / M_m of equation (24) by G_f / G_m, the shear modulus ratio of the two phases.

(c) Stiffness estimate transverse to fiber direction

The transverse modulus E_T can be approximated in the same way as continuous fiber composites namely using equation (23-25) and set the ratio l/d = 1.0

$$\frac{M_T}{M_m} = \frac{1 + ABV_f}{1 - B\psi V_f} \qquad (31)$$

where A = 2

It was pointed out that the Halpin-Tsai equation predicts that the transverse modulus of an aligned short-fiber composite is not influenced by the fiber aspect ratio (l/d) and its value is the same as that for the transverse modulus of a continuous-fiber composite. It is primarily the longitudinal modulus, E_L that is sensitive to l/d. The strong dependence of E_L on l/d ratio has been demonstrated and shown to be in good accord with theoretical predictions [7].

2.5 Flake-filled polymers

Flakes are especially effective in increasing the moduli of composites. Typical flake fillers include mica, kaolin, graphite, glass flakes, aluminum flakes, and aluminum diboride [2, 15-16]. Such materials support the constraints in all direction in a plane of reinforcement, and often have the behavior of biaxially oriented materials. Unlike fiber, materials with planar orientation of the flakes provide reinforcement with high strength and stiffness in two directions: the longitudinal direction and the in-plane transverse direction, i.e. typically a direction perpendicular to the length of the flakes in the plane of

the film or sheet. Materials with planar orientation of flakes have extremely high resistance to the permeation of gases and liquids. The addition of platelet fillers distributed in the polymer film can greatly increase the diffusion pathway; permeating molecules are forced to go around impermeable flakes creating a tortuous path for the diffusing species. The use of mica in ethylene vinyl alcohol (EVOH) copolymers was reported to show a threefold increase in oxygen barrier properties [4]. In addition, composite barrier performance was shown to be proportional to its filler aspect ratio.

Understanding the mechanism involved in flake reinforcement in composites has been mainly developed from a knowledge of fiber reinforced composite [3,5-6]. Polymers filled with flakes have characteristics analogous to short-fiber filled composites in which the stresses are transferred from the matrix to the fibers by shear stress at the matrix interface. Equation (29) holds for Young's modulus measured parallel to the flake's surface except that the constant A becomes [2];

$$A = 1.33\left(\frac{L}{t}\right)^{0.645} \qquad (32)$$

where L/t is the aspect ratio of the flakes, that is, their length divided by their thickness.

2.6 Reinforcement of rubber by fillers

In most application, rubber is normally modified by incorporation of fillers to modify properties so that acceptable engineering properties are obtained. The main filler classifications are carbon black, mineral products such as kaolin and calcium carbonate. The selection of filler used in rubber formulation is made based on the property requirement of the end-product. Typically carbon black would be used to enhance

strength characteristics while mineral fillers provide a more modest strength enhancement at significantly reduced cost [17].

A wide range of nonblack, particulate fillers is added to rubber compounds to improve the cured physical properties, reduced cost, and impart color to the rubber product. The chemical composition and its effect in rubber compound physical properties typically result in classifying particulate fillers into three broad categories [18]:

1. Non-reinforcing or degrading fillers
2. Semi-reinforcing or extending fillers
3. Reinforcing fillers

The term “reinforcement” refers to an improvement in end-use performance of the rubber compound associated with an increase in modulus and in the so-called ultimate properties including tensile strength, tear resistance and abrasion resistance. A reinforcing filler is a particulate material that is able to increase: (1) the tensile strength; (2) the tear strength; and (3) the abrasion resistance of natural rubber. A semi-reinforcing filler is a particulate material that is able to increase: (1) the tensile strength; and (2) the tear strength, but does not improve abrasion resistance. A non reinforcing filler is unable to provide any increase on these properties and functions only as a diluent [19].

2.7 Mineral fillers

Clays represent the largest volume nonblack filler used in rubber [20]. They are second to carbon black in this respect. Clay minerals are widely used in rubber because of their cost effectiveness in terms of providing beneficial reinforcing and processing properties at a modest cost. The main clay mineral of importance is kaolin (china clay)

and the derivative produced by chemical treatment and heating (calcining). Clay is classified as a hard clay if it reinforces rubber and also imparts high modulus, tensile strength, and resistance to abrasion. Clay is considered "soft" if it produced compound with lower physical properties.

Several commercial clays have been treated with silane coupling agents to improve their performance in rubber. Since the silane coupling agent provides a means to bond the clay particles to the rubber, increased modulus and tensile strength are obtained. Clay can be formulated to rather high loadings in most elastomers, with soft clays allowing somewhat higher loadings than hard clays. Viscosity builds moderately with loading, but processible formulations with 150-200 phr (part per hundred rubber) are reported to be feasible [21]. The main factor to consider in adding clay to most formulations is its reduction of cure rate. This reduction will require the addition of an activator and increase in accelerator system.

2.7.1 Kaolinite clay

Kaolinite clay is a widely used white filler in the rubber industry [22]. Depending on particle size, it can be used as a semi-reinforcing filler (hard clay) or a non-reinforcing filler (soft clay) in which they produce harder and softer rubber compounds, respectively. Application include chemical liners, bicycle tyres, conveyor belts, shoe soles, gasket and flooring where good reinforcement, moderate cost, and good processability are desired. Clays are commonly added to rubber compounds at levels of 20 to 150 phr.

Pure kaolinite has the idealized chemical composition $Si_2Al_2O_5(OH)_4$. It is a crystalline material with a triclinic form found in microscopic pseudo-hexagonal plates [19]. The inability of kaolinite crystals to show interlayer (intracrystalline) expansion or

swelling is indicative of strong interlayer bonding. The forces holding the layers together have been attributed to O-H---O hydrogen bonding [23]. Figure 2.3 illustrate the layer structure of kaolinite clay assembled as a 1:1 layer silicate. Its structure can be regarded as a gibbsite $Al(OH)_3$ layer bonded to a siloxane (Si_2O_5) layer. The Si atom in the siloxane layer is tetrahedrally bound to four oxygen atoms and the Al atom in the gibbsite grouping completes its favored octahedral environment by coordinating to two oxygen atoms in the siloxane group. Therefore, one face of this structure is comprised of oxygens and hydroxyl and the other hydroxyl groups. These will interact through hydrogen bonding giving a layered kaolinite crystals, which has a pseudo-hexagonal platy shape. These thin, hexagonal plates have aspect ratios in the range of 5:1 to 50:1, which are dependent on particle size.

In the latex industry, kaolinite clays are commonly incorporated in latex compounds. They are added dry to a well-stabilized latex or dispersed in water with the aid of small amounts of dispersing agents. Kaolinite clays may be added to natural rubber latex to the extent of 400 parts per 100 parts of rubber. The products at those levels are very hard and show virtually no rubbery characteristics. In low proportion (up to 30 parts per 100 parts of rubber), soft vulcanizates are obtained which have an increased tension set [24].

It has been argued that the reinforcing effect of inorganic fillers in dry rubber is not analogous to the reinforcement observed when the same fillers are incorporated in latex. Therefore carbon black and fine-particle kaolinite clays do not enhance the tensile strength and tear strength of vulcanized latex deposits as they do for products made from dry rubber. This difference is believed to be associated with the absence of a mastication

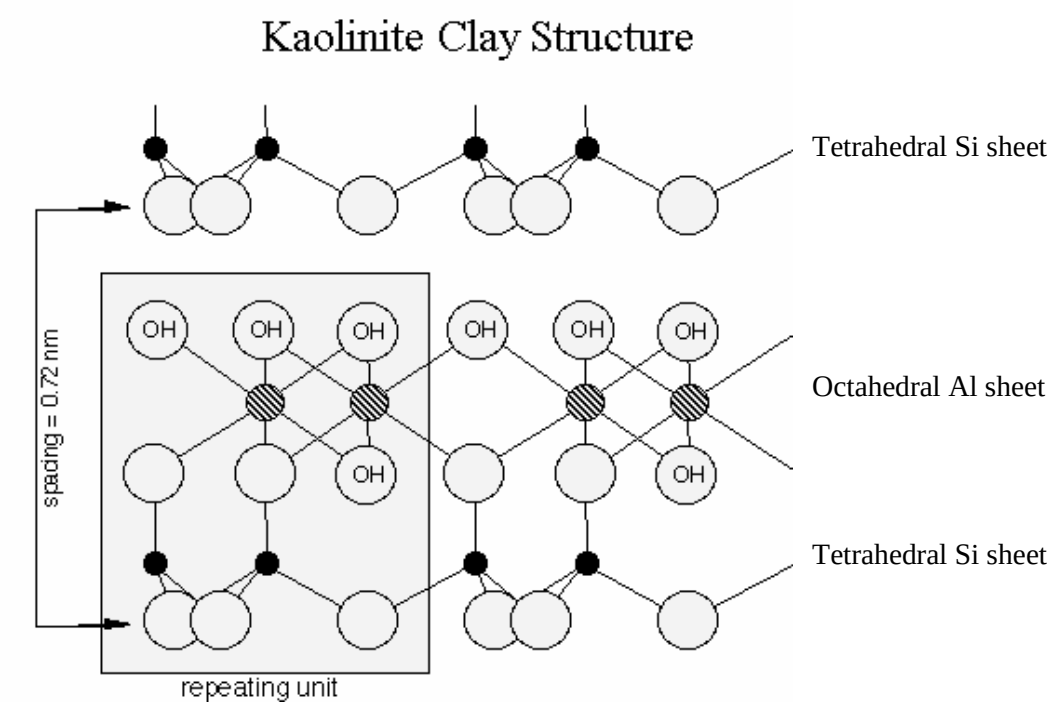

Figure 2.3 Schematic representation of a silica tetrahedral sheet and an octahedral Al hydroxide sheet. The layer structure of kaolinite along the a-axis. The basal or d (001) spacing of ~0.7 nm is equal to the layer thickness [23].

step in latex products. Mastication is a rigorous mechanical process that can cleave polymer molecules so that polymeric free radicals are produced. These radicals are able to interact with reactive sites on the surface of filler particles and hence improve adhesion, and increase strength considerably [24].

2.7.2 Montmorillonite

Montmorillonite has been reported to be used to control viscosity or impart thixotropy to a variety of liquid polymers based on unsaturated polyesters, PVC plastisols, polysulphides and, alkyds. In addition, montmorillonites are also used to control the melt rheology of thermoplastics and to reinforce polyamides [19].

The montmorillonite group comprises a number of clay minerals within the dioctahedral smectite group. The startling property of montmorillonite is its ability to expand and contract its interlayer structure while maintaining two-dimensional crystallographic integrity. By this means, a large active surface area (700-800 m^2 /g) is potentially exposed, allowing an enormous range of guest molecules to be intercalated [23]. Expansion takes place as water or some polar organic compound, such as ethylene glycol, enters the interlayer space. When montmorillonite expands, the interlayer cation may be replaced by other cations, therefore the cation-exchange capacities (CEC) of montmorillonite groups are high compared to other clay minerals that do not expand.

Montmorillonite belongs to the 2:1 type phyllosilicates, or layer silicates [25]. All layer silicates are basically composed of two modular units: A sheet of corner-linked silica tetrahedra and a sheet of edge-linked octahedra. These are joined together in varying proportions and stacked on top of each other. A schematic of how the 2:1 clay minerals can be assembled is shown in figure 2.4. Two tetrahedral sheets to one

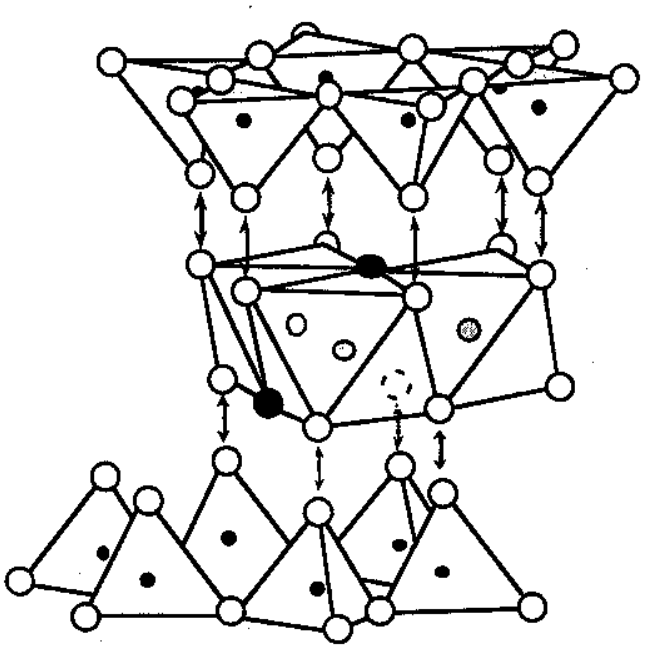

Figure 2.4 Three dimensional polyhedra showing how a 2:1 layer silicate can be imagined assembling. Large black circles are hydroxyl; small black circles are tetrahedrally coordinated cations; shaded circles are octahedrally coordinated cations; and open circles are oxygens [26].

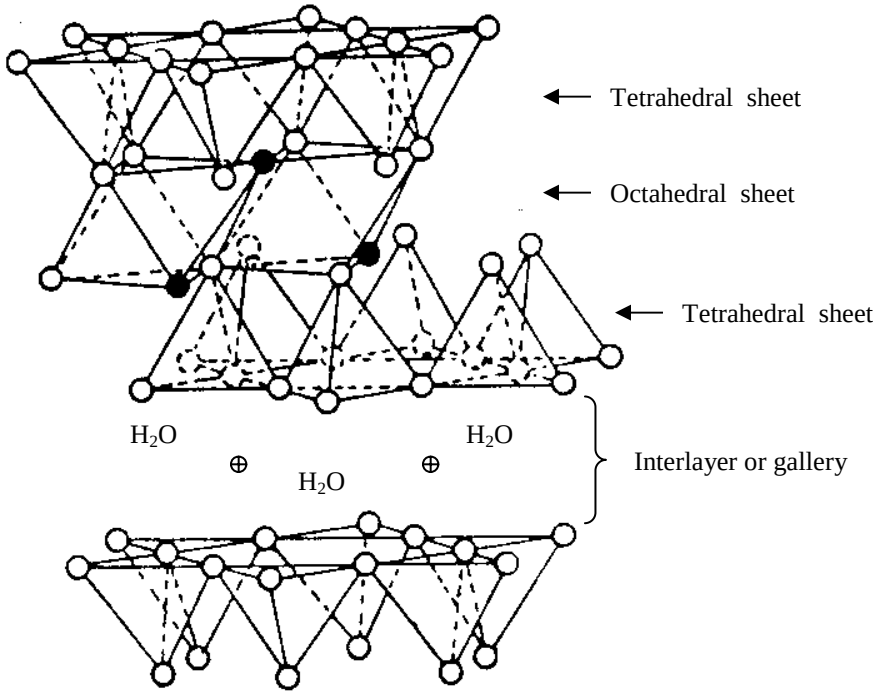

Figure 2.5 Idealized structure of 2:1 layered silicates showing two tetrahedral-site sheets fused to an octahedral–site sheet. Open circles represent oxygens; black circles are hydroxyls. The galleries in the pristine silicates are usually occupied by hydrated alkali metal cations [27].

octahedral sheet is formed by inverting a tetrahedral sheet, bring it down on top of the 1:1 layer (the lower plane of an octahedral sheet and a tetrahedral sheet) and replacing two-third of the hydroxyls with apical oxygen ions. This assemblage makes a tetrahedral-octahedral-tetrahedral sandwich. Montmorillonite has the origin of its layer charge primarily in the octahedral sheet. Substitution by ions of lesser charge, notably Si^{4+} by Al^{3+} in tetrahedral positions and Al^{3+} or Fe^{3+} by Mg^{2+} or Fe^{2+} in octahedral positions, results in negative charges on the interlayer space which are balanced by interlayer cations; commonly Na^{+}, Ca^{2+} and Mg^{2+} ions, but a wide range of other cations, including organic ions, can be introduced by exchanged reactions. Figure 2.5 shows the idealized layer structure of montmorillonite and the occupancy of the interlayer space by exchangeable cations as monovalent ions.

2.8 Filler Characteristics

As previously noted the reinforcing ability of a filler is influenced by three primary characteristics [19,28]: particle size, structure and surface activity (polymer–filler bonding).

(1) Particle size

Improvement in the physical properties are directly related to filler particle size. The increase of modulus and tensile strength is very much dependent on the particle size of the filler; smaller particulate fillers imparting greater reinforcement to the rubber compound than the coarse ones. Since particle size is directly related to the reciprocal of surface area per gram of filler, it is the increase in surface area that is in contact with the rubber phase which probably leads to the increase in reinforcement. Reducing particle

size also simply results in a greater influence of polymer-filler interaction. In addition to average particle size, the particle-size distribution also has a significant effect on reinforcement. Particulate fillers with a broad particle-size distribution have better packing in the rubber matrix, which results in a lower viscosity than that provided by an equal volume of filler with a narrow particle-size distribution. Another important concern in reinforcement is the presence of large particles or agglomerates in the rubber. These agglomerates not only reduce the contact between filler and matrix but function as failure initiation sites which would lead to premature failure of materials.

(2) Particle Structure and anisometry of filler aggregate

In addition to the surface area, the shape of the filler particle is an important factor that affects the performance of a rubber compound. Inorganic and mineral fillers posses considerable differences in particle geometry, depending on the crystal form of the mineral. The minimum anisometry is found with materials that form crystals with approximately equal dimension in the three directions, i.e. isometric particles. More anisometric are particles in which one dimension is much smaller than the two others, i.e. platelets. The most anisometric are particles which have two dimensions much smaller than the third, so that they are rod–shaped. In compounds containing fillers with identical surface area and chemical nature but different shape, modulus increases with increasing anisometry [29]. Particles with a high aspect ratio, such as platelets or fibrous particles, have a higher surface-to volume ratio, which results in higher reinforcement of the rubber compound. The greatest hardness is also provided by rod-shaped or plate-like particles, which can line up parallel to one another during processing, compared to spherical

particles of similar diameter. Particle shape has a more pronounced effect on processing behavior than on reinforcement and provides important benefits in this area. It can also significantly increase modulus due to occlusion or shielding of some of the rubber phase in highly structured fillers such as structural aggregates of carbon black or silica [30].

(3) Surface activity

The particle size of the filler as discussed earlier may be considered as a physical contribution to reinforcement, while filler surface activity provides the chemical contribution. The ability of the filler to react with the polymer results in bonding, which increases strength significantly. In the absence of strong coupling bonds, the polymer is physically absorbed on the surface of the filler, resulting in a reduced mobility of the rubber molecules near the surface of the filler. Polymer-filler bonding, particularly in the case of carbon black, develops through active sites on the filler surface resulting in '**bound rubber**' attached to the filler surface. The effect of these surface interactions has been demonstrated by comparing the effect of using carbon black before and after graphitization (heat treatment of the carbon black to a temperature of 1600-3000 °C). Through this treatment the activity of the sites is lost and the amount of bound rubber (rubber unextractable from the unvulcanized mix) drops dramatically. The disappearance of active sites for physical absorption has the most profound effect on the mechanical properties of the compound made with this black. Bound rubber is regarded as the result of rubber to filler interactions which can be considered as a measure of the surface activity of the black or white filler and therefore, is reflected in the rubber properties related to surface activity such as modulus, abrasion and tear resistance [31].

Adhesion between polymer and filler may also be induced by a coupling agent, which participates in the vulcanization reaction to form polymer-filler crosslinks. This mechanism of increasing strength is well established with both mineral fillers and carbon blacks [19]. Both mechanisms lead to the formation of high modulus compounds, which is a very clear indicator that polymer-filler bonding has taken place. The increased modulus occurs as a direct result of attachment of the rubber to the filler, which has the effect of reducing polymer mobility. Organo silane coupling agents have been successfully utilized to further increase the physical properties of a number of non-black fillers including calcium silicate, clay, mica, silica, and talc [20].

2.9 Effect of filler properties on the effective volume in the filled rubber

Since fillers are classified on the basis of their particle size, structure and surface activity as discussed above, these parameters influence effective filler volume in the filled system in different ways. It has been reported that the filler volume fraction in a polymer system behaves in many aspects – such as rheological properties of the compound, static stress-strain behavior of the vulcanizate, and dynamic viscoelastic response – as if its concentration is much higher than its real volume fraction based on its density and loading. An effective volume fraction (instead of real volume fraction) has been used to describe the effect of filler on rubber properties [29].

The concept of immobilized **occluded rubber** has been used by several authors to account for the effect of carbon black structure on viscoelastic properties [30,32-33]. Rubber trapped in the internal void volume of filler aggregates and agglomerates is

immobilized and totally or partially shielded against deformation. The effective immobilization of this rubber portion, acting as part of the filler rather than of the polymer matrix, increases the effectiveness of the filler beyond the value calculated from the mass and density of the filler. The increase in modulus of rubber may be regarded as a hydrodynamic effect in which the effective volume of carbon black is increased by occluded rubber. Therefore, the modulus of the filled rubber should reflect the effect of filler morphology (particle size and structure) and surface activity as stated earlier, which determines filler-polymer and aggregate-aggregate interaction.

It has also been shown that depending on the strength of polymer-filler interactions, physical adsorption and/or chemisorption of rubber molecules may take place on the filler surface. This interaction leads to an effective immobilization of the elastomer segments (**immobilized rubber**). Depending on the intensity of the filler-polymer interaction and the distance from the filler surface, the mobility of the polymer segments near the interface is lower than that of in the matrix. The proposed rubber shell model demonstrated the presence of three distinct regions within the polymer characterized by different degrees of molecular mobility [30,34]: a region of mobile rubber, an outer shell surrounding the carbon black which is less mobile, and a hard inner shell where the motion of rubber molecules is extremely restricted. In general, it is assumed that the modulus of the inner shell is very high and decreases gradually with increasing distance from the filler surface. The amount of rubber in this volume of the shell obviously depends on polymer-filler interaction and the surface area of the filler. Therefore, filler surface activity or surface energy, and its particle size may be considered as factors influencing the effective volume of the filler.

Note that occluded rubber is not synonymous with bound or immobilized rubber, though obviously some portion of the occluded rubber is both [30].

There has been considerable evidence supporting the tendency of filler aggregates to associate to form agglomerates, especially at high filler loading [35-37]. This leads to a chain-like filler structure or clusters termed as **secondary structure** or **filler network**, which may be described as poor micro-dispersion. Filler-filler interaction and the rubber trapped in the secondary structure which is not destroyed during deformation may noticeably increase the effective filler volume fraction, leading to high elastic modulus for the filled rubber compound. The formation of a secondary filler network and its strength are governed by attractive forces between aggregates, the degree of polymer-filler interaction and the distance between aggregates. A large difference in surface energy between filler and polymer and short interaggregate distance could result in high agglomeration. The appearance or detection of agglomerates was derived from measurement of dynamic properties. This agglomeration is highly strain and temperature-dependent. At moderate and high strain, breakdown of the filler network would release trapped rubber so that the effective filler volume fraction and hence, the modulus would decrease. On the other hand, raising the temperature would weaken interaggregate interaction resulting in reduced filler agglomeration. Filler networks are more developed and stronger at low temperatures.

2.10 Hydrodynamic model of rubber-filled system

Theoretical models dealing with the effects of particulate fillers on the mechanical properties of rubber have long been demonstrated primarily with carbon black. The

model for predicting elastic moduli of filled rubber has been developed from suspension rheology via a relative change in viscosity.

Experimentally when we dispersed rigid particles into a fluid, either a liquid or an elastomer, there is an increase of the viscosity in the case of the liquid or of the modulus in the case of an elastomeric polymer matrix.

Early investigations carried out to explain the reinforcing effect of colloidal fillers in elastomers were based on Einstein's viscosity equation. The viscosity of a colloidal suspension can be described by hydrodynamic analysis [38,39], and the now well known viscosity law,

$$\eta = \eta_0 (1 + 2.5\phi) \qquad (33)$$

This hold only for rigid spherical particles that are well wetted by the polymer and have negligible particle-particle interaction. Where ϕ is the volumetric concentration of filler and η_0 and η are the viscosity of the pure liquid and of the suspension respectively. Equation (33) is applied to the modulus of a filled elastomer,

$$E = E_0 (1 + 2.5\phi) \qquad (34)$$

Where E is Young's modulus which can be applied at small deformations to elastomers filled with small quantities of spherical fillers. In order to take into account interaction between filler particles Guth [40] introduced a quadratic term and obtained equation (35). It was thus possible to describe the stress-strain behavior of vulcanizates filled with spherical fillers over a wide range of filler loadings;

$$E = E_0 (1 + 2.5\phi + 14.1\phi^2) \qquad (35)$$

We take into account the influence of particle shape, which always departs from the perfect spherical shape, by introducing a shape factor, f to account for the anisotropy of colloidal particles. The shape factor is the ratio of the longest dimension of the particle to the shortest, that is the ratio of length over diameter of rod-shaped particles.

$$E = E_0(1 + 0.67\, f\phi + 1.62\, f^2\phi^2) \qquad (36)$$

Remembering the occluded rubber trapped in the internal void volume of the filler aggregates and agglomerates, and the assumption that occluded rubber is shielded from deformation and acts a part of the filler, Medalia [33] replaced the volume fraction ϕ in equation (35) by an effective volume fraction ϕ_{eff}.

$$E = E_0(1 + 2.5\phi_{eff} + 14.1\phi_{eff}^{\ 2}) \qquad (37)$$

Where

$$\phi_{eff} = f\phi \qquad (38)$$

The value of ϕ_{eff} can be estimated directly using dibutyl phthalate (DBP) absorption, which fills the voids between particles. Since shielding is not fully effective, an occlusion effectiveness factor was introduced to fit the experimental data. It has also been suggested that bound rubber should be considered as part of the volume occupied by the filler since this would influence hydrodynamic properties, such as viscosity of the filled compound [41].

It was pointed out by Nielsen [2] that the prediction of moduli from a viscosity relationship is inaccurate since the viscosity ratio is often larger than the modulus ratio. However, a simple relationship between relative viscosities and relative moduli is valid for filled systems in which the matrix phase is an elastomer having a Poisson's ratio of 0.5, and the filler phase is rigid.

Following the above discussion it is evident that the effects of individual filler parameters on the effective filler volume are associated with different mechanisms. The change in mechanical and dynamic properties due to filler presence in a rubber compound being the result of first, a hydrodynamic effect, and then the influence of different kinds of interactions (polymer to filler surface and filler to filler surface interactions).

REFERENCES

1. Agarwal, B. D. and Broutman, L. J. (1990), Analysis and Performance of Fiber Composites, 2 nd. ed., Wiley, New York, 448 pp.
2. Nielsen, L. E. and Landel, R. F. (1994), Mechanical Properties of Polymers and Composites, 2 nd. ed., Marcel Dekker, New York, 545pp.
3. Rexer, J. and Anderson, E. (1979), Composites with Planar Reinforcements (Flake, Ribbons)- A Review, Polymer Eng. Sci.,19,1.
4. Bissot, T. C., Performance of High – Barrier Resins with Platelet- Type Fillers, American Chemical Society, Symposium Series, vol. 423, American Chemical Society, Washington DC, 1990.
5. Maine, F. W. and Shephed, P. D. (1974), Mica Reinforced Plastics: A Review, Composites, 5, 193.
6. Padawer, G. E. and Beecher, N. (1970), On the Strength and Stiffness of Planar Reinforced Plastics Resins, Polymer Eng. Sci., 10, 185.
7. Halpin, J. C. (1969), Stiffness and Expansion Estimate for Oriented Short Fiber Composites, J. Composite Materials, 3, 732.
8. Halpin, J. C. (1969), Primer on Composite Materials Analysis, 2 nd. ed, Technomic, Lancaster, Pa., 227 pp.
9. Halpin, J. C. and Kardos, J. L. (1976), The Halpin-Tsai Equation: A Review, Polymer Eng. Sci., 16(5), 344.
10. Tsai, S. W. (1968), Formulus for the Elastic Properties of Fiber-Reinforced Composites, U. S. Dept. Commerce Rept. AD834851.

11. Nielsen, L. E. (1970), Generalized equation for the Elastic Moduli of Composite Materials, J. of Applied Physics, 41(11), 4626.
12. Katz, H. S. and Milewski, J. V., editors (1978), Handbook of Fillers and Reinforcements for Plastics, Van Nostrand Reinhold Co., New York, 652pp.
13. Chow, T. S. (1980), Review the Effect of Particle Shape on the Mechanical Properties of Filled Polymers, J. of Materials Science, 15, 1873.
14. Lusis, J., Woodhams, R. T. and Xanthos, M. (1973), The Effect of Flake Aspect Ratio on the Flexural Properties of Mica Reinforced Plastics, Polymer Eng. Sci., 13, 139.
15. Newman, S. and Meyer, F. J. (1980), Mica Composites of Improved Strength, Polymer Composites, 1(1), 37.
16. Okuno, K. and Woodhams, R. T. (1975), Mica Reinforced Polypropylene, Polymer Eng. Sci, 15(4), 308.
17. Katz, H. S. and Milewski, J. V. (1987) Handbook of Fillers and Plastics, Van Nostrand Reinhold Co., New York, 459pp.
18. Dick, J. S., Editor (2001) Rubber Technology: Compounding and Testing for Performance, Hanser Publishers, 523 pp.
19. Rothon, R., Editor (1995) Particulate-Filled Polymer Composites, Longman Scientific & Technical, New York, 371 pp.
20. Morton, M., Editor (1987) Rubber Technology, 3 ed., Van Nostrand Reinhold Co., New York, 631 pp.
21. Bateman, L. (1963) Chemistry and Physics of Rubber-like Substances, John Wiley & Sons, 777 pp.

22. Kraus, G., Editor (1965) Reinforcement of Elastomers, Interscience Publishers, New York, 605 pp.
23. Theng, B. K. G. (1979) Formation and Properties of Clay-Polymer Complexes, Elsevier Scientific Publishing Company, New York, 353 pp.
24. Blackley, D. C. (1966) High Polymer Lattices; Their Science and Technology: Volume 1 Fundamental Principles, Palmerton Publishing Co., New york, 351 pp.
25. Brindley, G. W., and Brown, G. (1980) Crystal Structure of Clay Minerals and their X-ray Identification, Mineralogical Society, 485 pp.
26. Moore, D. M. and Reynolds, R. C., Jr. (1989) X-ray Diffraction and the Identification and Analysis of Clay Minerals: Oxford University Press, Oxford, 332 pp.
27. Giannelis, E. P. (1996) Advanced Materials, 8, No. 1, 29-35.
28. Blow, C. M., Editor (1971) Rubber Technology and Manufacture, The Chemical Rubber Co., Ohio, 509 pp.
29. Wang, M. J. (1998) "Effect of Polymer-Filler and Filler-Filler Interactions on Dynamic Properties of Filled Vulcanizates", Rubb Chem Technol, 71, 520-583.
30. Eirich, F. R., Editor (1978) Science and Technology of Rubber, Academic Press, New York, 633 pp.
31. Wolff, S. (1996) "Chemical Aspects of Rubber Reinforcement by Fillers", Rubb Chem Technol, 69, 325-346.
32. Medalia, A. I. (1987) "Effect of Carbon Black on Ultimate Properties of Rubber Vulcanizates", Rubb Chem Technol, 60, 45-61.
33. Medalia, A. I. (1972) "Effective Degree of Immobilization of Rubber Occluded within Carbon Black Aggregates", Rubb Chem Technol, 45, 1171-1194.

34. Wolff, S. and Wang, M. J. (1992) “Filler-Elastomer Interactions Part IV the Effect of the Surface Energies of Fillers on Elastomer Reinforcement”, Rubb Chem Technol, 65, 329-342.
35. Wang, M. J., Wolff, S. and Tan, E. W. (1993) “Filler-Elastomer Interactions; Part VIII the Role of the Distance between Filler Aggregates in the Dynamic Properties of Filled Vulcanizates”, Rubb Chem Technol, 66, 178-195.
36. Wang, M. J. (1999) “The Role of Filler Networking in Dynamic Properties of Filled Rubber”, Rubb Chem Technol, 72, 430-447.
37. Payne, A. R. (1965) Reinforcement of Elastomers, Kraus, Ed., Interscience Publishers, New York, Ch.3.
38. Wolff, S. (1990) “Characterization of Fillers in Vulcanizates According to the Einstein-Guth-Gold Equation”, Rubb Chem Technol, 63, 32-45.
39. Donnet, J. B. (1998) “Black and White Fillers and Tire Compound”, Rubb Chem Technol, 71, 323-339.
40. Guth, E. (1945) “Theory of Filler Reinforcement”, J. Appl Phys, 16, 20-25.
41. Dannenberg, E. M. (1986) “Bound Rubber and Carbon Black Reinforcement”, Rubb Chem Technol, 59, 512-524.

CHAPTER 3

EXPERIMENTAL

3.1 Introduction

This chapter details the preparation and characterization of natural rubber latex/montmorillonite clay composites. The mechanical properties of composite films were determined using Instron static mechanical testing. X-ray diffraction was used to characterize the structure of polymer-silicate composites and to explore the extent of the dispersion of clays in the filled samples. The water vapor-barrier performance of the composite films was measured using a standard test method to observe the anticipated benefit of dispersing large aspect ratio silicate layers into the rubber matrix.

3.2 Materials

Sodium montmorillonite, supplied by Southern Clay Products [1] was used in this work as a pristine silicate. Kaolin with an average particle size of 0.1-4 microns was received from Aldrich. Commercial low ammonia NR latex concentrate (Firestone Hartex®101) prepared by centrifugation, was used as received. The preservative system in the latex consists of a low ammonia concentration in combination with 0.036% tetramethylthiuram disulphide and 0.036% zinc oxide, expressed as a wet weight basis. The dry rubber content (DRC) of the latex is 61.15% (w/w). Typical properties of Hartex®101 according to literature are shown in table 3.1.

Table 3.1 Properties of Hartex®101 [2].

Properties	
Total Solid Content, %	62.31
Dry Rubber Content, %	61.15
Total Alkalinity, %NH3 on wet weight	0.25
KOH number	0.48
Mechanical Stability, sec.	1440
Volatile fatty Acid (VFA) number	0.008
pH	10.02
Sludge Content, % on wet weight	0.004
Coagulum, %	0.02

The graft polymer latex was kindly supplied by Heveatex Corporation, MA. It is made by polymerizing methyl methacrylate monomer in the presence of natural-rubber latex. The polymethylmethacrylate (PMMA) chains are thereby grafted to the rubber molecules. The latex contains 30% PMMA with total solids content of 50±1.5%.

3.3 Sample preparation

The clay loading used in a natural rubber (NR) latex/ montmorillonite (MMT) composites was 5 wt% and 10 wt% for tensile test and 50 wt% for XRD analysis. Composite film samples were prepared by stirring the latex with a desired amount of clay at room temperature for 12 hours. To obtain a proper film, latex-montmorillonite mixtures were diluted with water to a concentration of 30%. Films were subsequently cast on petridish by drying the mixture at 25°C for 12 hours under ambient pressure, then under vacuum for an additional 24 hours. Ground films were made into pellets for XRD

experiments. Mechanical properties were tested on a dog-bone die cut samples. These samples were kept in desiccator at all time before further analysis.

3.4 Characterization techniques

3.4.1 X-ray diffraction

Wide-angle x-ray diffraction (XRD) was used to examine the extent of dispersion of clay in filled samples. XRD patterns were obtained on the Scintag Pad V theta-2 theta goniometer with Si(Li) Peltier detector, using CuKα radiation with wavelength λ=1.540562 angstroms. Typical power settings are 30 mA and 35 kV. The scan range is 2-30 degree with a scan rate of 0.5 degree/min.

3.4.1.1 Processing of the x-ray raw data

The steps involved in data work-up analysis are as follows and use existing XRD instrument software.

(1) The 001 reflection of the montmorillonite was chosen for analysis

(2) This diffraction peak is smoothed using a simple box car averaging algorithm. The number of points in the box car determines the amount of smoothing, larger number of points cause more smoothing. All data analyzed have been smoothed using 9 points.

(3) The peak shape was corrected for a theta-dependent function, namely the Lorentz-polarization factor (see appendix) which results from diffraction and the use of a non-monochromatic divergent radiation source.

(4) The peak profile was then modeled using a mathematical function available with the instrument software. A split-Pearson VII curve type (see appendix) was selected since this function created the best fit of the peak's shape, providing minimum residual error. Fitting is an iterative process with the number of iterations specified to be ≈ 30 for profile refinement. The curve fitting routine stops when the error for the peak profile fit is less than 0.01%, or if the fit fails to converge after the number of specified iterations on the profile fitting program. Any intermediate results that are an improvement are displayed. All the peak positions and intensities are recorded.

(5) An instrument standard is also analyzed and its peak modeled in exactly the same manner as the sample. The observed sample peak breadth is then corrected for machine broadening as follows

$$B^2 = B(obs)^2 - b^2 \qquad (3.1)$$

Where:

B (obs) is the measured breadth at half height for the sample's peak

b is the breadth at half height for instrument standard and

B is the "corrected" breadth at half height

3.4.1.2 Determination of crystal size and number of diffracting layers from x-ray line broadening

Thickness of crystal or, particle-size broadening is conveniently inferred from the width of a peak at half- height. This is expressed quantitatively by the Scherrer equation [3].

$$L = \lambda K / B \cos\theta \qquad (3.2)$$

Where:

L = mean crystallite dimension in Angstrom along a line normal to the reflecting plane

K = a constant near unity and related to crystallite shape. For most purposes it suffices to take the constant K as unity; although a more accurate value for clay is 0.91 [4].

λ = wavelength of radiation used (1.540562 angstroms for CuKα)

B = the corrected breadth of the XRD peak at half-height expressed in radians on the 2θ scale (measure 2θ in degrees and then multiply by π/180)

Equation (3.2) can be directly applied if no other factors affect the measured breadth of the diffraction peak. However, the angular breadth is always affected by the design of the x-ray powder camera or diffractometer. A correction for instrumental effects is obtained approximately by the following relation [5];

for Gaussian profiles $B(obs)^2 = B^2 + b^2$ (3.3)

and for all Cauchy profiles $B(obs) = B + b$ (3.4)

Where:

B (obs) = the experimentally measured breadth at half-height for the sample's peak

B = corrected breadth to be used in equation (3.2)

b = breadth arising from instrumental effects

The value of b is estimated by using a standard material that contains no defects, strain, or particle size broadening. Theoretically, such a material produces narrow diffraction lines whose profiles are only broadened by instrument distortions.

In order to determine the number of layers in a crystal (N), the breadth of the basal 001 reflection was measured. Then, after making the appropriate correction for instrumental broadening, a value of L can be obtained using equation (3.2) and the number of layers in the crystal will be given by L/d(001). All of these analyses ignore any effects due to distributions of crystal thickness and so called type I or type II lattice distortions. As is the case with most polymer systems we don't observe enough reflections to correct for these lattice effects.

3.4.2 Tensile properties determination

Tensile properties were obtained using an Instron Static Mechanical Tester (model 4201) on dog-bone-shaped die-cut samples according to ASTM D1708, samples have a gauge length of 22 mm and a width of 5 mm. Grips were air activated with flat faces that were surfaced with emory cloth in order to prevent slippage of the specimen during testing which could lead to errors in elongation measurement. Ten specimens were cut and their thickness were determined with a Fowler micrometer having resolution of 0.0025 mm (0.0001in). Thickness was taken at three different places on the specimen and averaged for modulus calculation. Samples were carefully mounted straight and symmetrically in the grips of the Instron tester and then were stressed at a constant strain rate of 50.00 mm/min until failure. Data collection was performed using an IBM model 30 personal computer with Instron series IX version 6.02 software. Young's modulus

was reported as the slope of the initial linear region of the stress-strain curve at 5% deformation. Actual experimental values were reported as load- deformation curves. Therefore the experimental curves require scale transformation to obtain the desired stress-strain curves. This can be accomplished by the following definitions [6];

$$\text{Stress } \sigma = \frac{\text{force or load F}}{\text{cross sectional area A}} \tag{3.5}$$

$$\text{Strain } \varepsilon = \frac{(L - L_0)}{L_0} \tag{3.6}$$

Lo is the original, unstretched length of the specimen

L is the stretched length of the specimen

Thus Young's modulus in a tensile test is given by

$$E = \frac{d\sigma}{d\varepsilon} \tag{3.7}$$

The end of the stress-strain curve denotes the rupture or failure of the material, which is characterized by the tensile strength, σ_B and the ultimate strain or elongation to break, ε_B.

3.5 Permeability measurement

Permeability of water in clay/latex film was studied using the desiccant method according to ASTM standard E 96-95. The purpose of this test is to see if barrier properties are improved in the system due to the presence of large aspect ratio silicate layers in the polymer (rubber) matrix.

Films containing 5% by weight montmorillonite were prepared and then sealed with silicone to the open mouth of a test dish containing desiccant (anhydrous calcium

sulfate). The assembly was placed in a controlled humidity chamber. Periodic weighing of the entire test assembly determined the rate of water vapor movement through the composite film.

Appendix:

I. Profile fitting of powder diffraction patterns

The primary objective of profile fitting is to fit a numerical function, specifically referred to as a profile-shape-function (PSF), to a measured diffraction line. A variety of PSFs employed on data collected with different radiation sources and in different instrumental geometries have been investigated in the literature. Table 1 lists several of the common PSFs used in profile fitting [7]. Profiles that have been used for x-ray studies include: the three forms of the Lorentzian (or Cauchy) function included the normal Lorentzian (exponent =-1), the intermediate Lorentzian (exponent =-1.5), the modified Lorentzian (exponent=-2), Voigt and pseudo-Voigt functions, and the Pearson VII function. The Gaussian profile is commonly used for neutron diffraction. The selected function is best-fit to the diffraction trace, usually by a least-squares method: and all the peak positions and intensities are recorded.

These PSFs are typically described by three parameters: (1) the line position, $2\theta_k$, (2) a peak or integrated line intensity, I_0, and (3) the line width expressed as the full-width at half-maximum intensity, FWHM or H_k . An optimization algorithm is employed to adjust the PSF's parameters until the difference between the measured and the calculated lines are minimized.

In general, the most widely used PSFs are the pseudo-Voigt or Voigt function and the Pearson VII function since their shape can vary between that of a Lorentzian and a Gaussian function.

The peak shape in x-ray diffraction pattern is a complex convolution of several sample and instrumental effects and therefore can vary significantly depending on the

data collection geometry and type of sample. As a consequence of many combined sample and instrumental effects which will be discussed below (section III), the shape of the Bragg peaks in a powder XRD pattern deviates significantly from Gaussian and give rise to pronounced asymmetry in the observed peak shape, especially at low diffraction angles. An elaborate profile fitting method is required to accurately describe the experimental profile.

Table 1. Analytical functions used in representing diffraction profiles [7].

Name	Function
Gaussian	$A_1 \exp\left(-\frac{x^2}{k_1^2}\right)$
Lorentzian	$A_2 (1+k_2^2 x^2)^{-1}$
Modified Lorentzian	$A_3 (1+k_3^2 x^2)^{-2}$
Intermediate Lorentzian	$A_4 (1+k_4^2 x^2)^{-1.5}$
Voigt	$A_5 \int_{-\infty}^{\infty} L(x') G(x-x') d(x')$
Pseudo-Voigt	$A_6 [wL(x) + (1-w) G(w)]$
Pearson VII	$A_7 [1+4(2^{1/m}-1) (x^2 / k_7^2)]^{-m}$

Where: $m = k'_7 + k''_7/2\theta + k'''_7 / (2\theta)^2$

$x = 2\theta_i - 2\theta_k$: the angular distance between the 2-theta point being calculated and the 2-theta position of the peak maximum

k_n are constants related to the half-width

A_n are normalizing constants

L and G are Lorentzian and Gaussian functions

P and Q are polynomials containing only even exponential terms

The Pearson VII function allows the values of N to be varied along with peak position, height, and width. The Pseudo-Voight function is the sum of a varying proportion of Lorentzian and Gaussian function.

II. Pearson VII as a profile shape function of X-ray data

Among the various mathematical functions describing peak-profile shape available with the instrument software, fitting peaks with split-Pearson VII profile yielded a better fit than did use of other profiles.

Brown and Edmonds [7] evaluated the Pearson VII function which can range from a basic Lorentzian to a Gaussian function. It is sometimes referred to in the literature as a "variable Lorentzian" due to its flexibility. When the exponent m =1, 1.5, 2, the function take the form of basic, intermediate, and modified Lorentzian, respectively. When m approaches infinity the Pearson VII function become equivalent to the Gaussian function. The value of m is most strongly related to the shape of the tails of the profiles as illustrated in figure 3.1. In practice, m=10 is sufficient to approximate the Guassian function.

The Pearson VII can be used as a single profile and as a split profile [8]. Split profile as illustrated in figure 3.2 use two "half-profiles" to generate a single asymmetric line profile. The two halves share a common Bragg, $2\theta_k$, and peak intensity, Io, allow for the modeling of asymmetric line shapes. The value of m and H_k on the low- and high-angle sides can be allowed to vary independently [9-11].

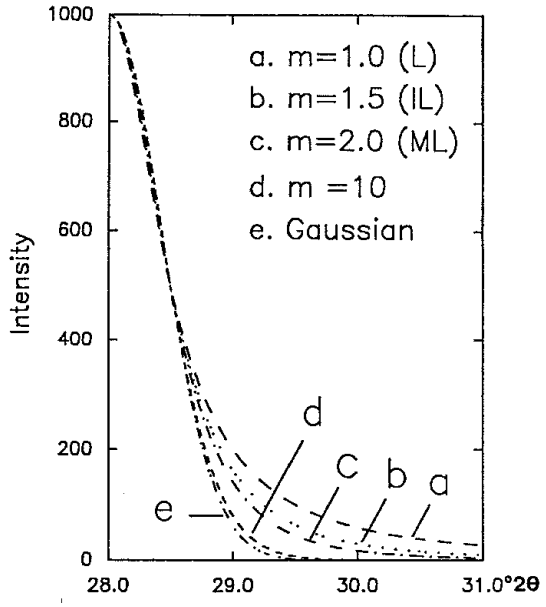

Figure 3.1 A series of Pearson VII profiles generated with the full-width at half – maximum but with different values of the exponent m. A Gaussian profile is also shown for comparison. Depending on the value of m, the function replicates the Intermediate (IL), Modified (ML), and Pure (L) Lorentzian profile. The shape of the profile is essentially Gaussian when m exceeds approximately 10 [8].

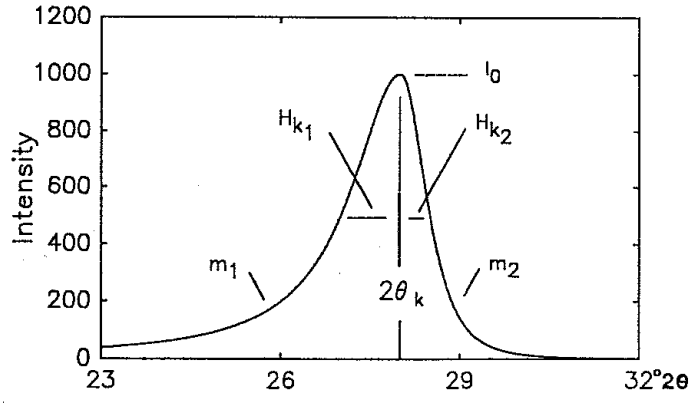

Figure 3.2 A split-Pearson VII profile. Two half profiles share a common Bragg angle, $2\theta_k$, and peak intensity, I_0. Their different full-widths at half maximum, H_k, and exponent, m, allow the profile to model an asymmetric line [8].

III. Factor that affect XRD peak broadening

There are four factors that primarily affect XRD peak breadth

1. Instrumental effects, which broaden all of the XRD peaks as a complicated function of diffraction angle. Klug and Alexander [5] identified six functions arising from a typical x- ray diffractometer that modify the pure Bragg diffraction peaks: (1) geometry of the x-ray source, (2) varying displacements of different portions of a flat sample surface from the focusing circle (flat-specimen error), (3) axial divergence of the x-ray beam, (4) specimen transparency, (5) effects of receiving slit, and (6) misalignment of diffractometer. It would be very complicated to remove independently each of these effects from the diffraction profile. However, these effects can be removed collectively by using an instrumental standard. The choice of a standard is not critical in this case, because clay peaks are so broad that the instrumental contribution to peak breadth generally is small [12].

2. Strain or distortion within a crystal, which broadens XRD peaks increasingly as a function of the order of the reflection. Strain causes peaks to shift from their ideal location in the unstrained state. Usually, there is a distribution of strain in a sample that results in a distribution of shifts that distorts the peak shape considerably. Strain is also invariably accompanied by the breakup of macrocrystallites into microdomains of different strain values that complicates the diffraction profile by superimposing broadening from the domains on the range of shifts caused by the range of strain values. Strain is defined as "change in length per unit length" and is measured as the change in d-spacing of a strained sample compared to the unstrained state.

3. Stacking faults or mixed-layering within crystals, which broaden different orders of reflection differently and often non-symmetrically, depending on the type of stacking fault. XRD peaks for a clay will be shifted and broadened by a coherently diffracting interlayering phase having a different d(001). The magnitude of this effect will depend on the d-value, quantity and ordering of the interlayering phase.
4. Crystallite size or x-ray scattering domain size, which is the quantity we are interested in measuring. Crystallite size broadens all peaks equally as a function of the order of the reflection, after the theta- dependent functions (such as the Lorentz-polarization and the structure factor) have been removed from the diffraction profile.

IV. The Lorentz-polarization (Lp) factors

The polarization factor accounts for increases in peak and background scattering from a maximum at 0° 2θ to a minimum at 90° 2θ. The basis for this change is that as radiation comes from the tube it is unpolarized, but the process of scattering causes a degree of polarization related to the angle of the incident and diffracted beam. The x-rays are polarized as they are diffracted from a plane of atoms. The polarization factor, $(1+\cos^2 2\theta)/2$, describes changes in intensity due to polarization of the x-ray beam during scattering.

The Lorentz factor is a combination of two geometrical factors. The first factor involves the volume of crystal that is exposed to primary irradiation. The second one relates the number of crystals favorably oriented for diffraction at any Bragg angle. The two portions of the Lorentz factor are combined with the polarization factor $(1+\cos^2 2\theta)/2$ and given in the following forms:

The Lorentz polarization (Lp) factor for integrated intensity from a randomly oriented powder [3,12],

$$Lp = \frac{1+\cos^2 2\theta}{\sin\theta \sin 2\theta} \qquad (I)$$

The Lorentz factor, which is the denominator of equation (I) is usually written $1/\sin^2\theta \cos\theta$ for random powders. Since $\sin 2\theta = 2 \sin\theta\cos\theta$, substituting the right hand side of this equation into the denominator of equation (I) for the quantity $\sin 2\theta$, the two forms of the Lorentz factor are identical except for the factor of 2, which can be neglected for studies involving relative intensities.

REFERENCES

1. Southern Clay Product data sheet.
2. Firestone Company Data Sheet.
3. Moore, D. M. and Reynolds, R. C., Jr. (1989) X-ray Diffraction and the Identification and Analysis of Clay Minerals: Oxford University Press, Oxford, 332 pp.
4. Brindley, G. W., and Brown, G. (1980) Crystal Structure of Clay Minerals and their X-ray Identification. Mineralogical Society, 485 pp.
5. Klug, H. P. and Alexander, L. E. (1974) X-ray Diffraction Procedures, 2 nd ed., John Wiley and Sons, New York. 923 pp.
6. Nielsen, L. E. and Landel, R. F. (1994) Mechanical Properties of Polymers and Composites, 2 nd ed, Marcel Dekker, Inc., 545 pp.
7. Brown, A. and Edmonds, J.W. (1980) The Fitting of Powder Diffraction Profiles to an Analytical Expression and the Influence of Line Broadening Factors. Adv. X-ray anal. 23, 361.
8. Howard, S. A. and Preston, K. D. (1989) Profile Fitting of Powder Diffraction Patterns: in Modern Powder Diffraction, D. L. Bish and J. E. Post, eds., Reviews in Mineralogy 20, Mineralogical Society of America, Washington, D.C., 217-276.
9. Brown, A. and Linde, S. (1987) Powder Diffraction Profiles and the Pearson VII Distribution, Advances in X-ray Analysis, 30, 343-350.
10. Gupta, S. K. (1998) Peak Decomposition Using Pearson Type VII Function, J. Appl. Cryst., 31, 474-476.
11. Hall, M. M. et al (1977) The Approximation of Symmetric X-ray Peaks by Pearson Type VII Distributions, J. Appl. Cryst., 10, 66-68.

12. Reynold, R. C., Jr. and walker, J. R. (1993) Computer Application to X-ray Powder Diffraction Analysis of Clay Minerals, The Clay Mineral Society, 155 pp.

CHAPTER 4

RESULTS & DISCUSSION

4.1 Introduction

The present chapter presents the characterization and properties of natural rubber latex / sodium montmorillonite composites formed in a water based latex system. Special attention has been paid to an investigation of the mechanical properties, particularly concerning the composite tensile modulus. Attention is also drawn to the relationship between the enhanced modulus values and the structure of the composites formed. Wide angle x-ray diffraction techniques were utilized to explore the extent of dispersion of clay in filled systems. Furthermore, the water vapor barrier properties of composite films were examined.

4.2 Mechanical properties

In this study, we make use of the hydrophilic nature of pristine sodium montmorillonite to allow dispersion of its inorganic crystalline layers in a watery suspension of rubber particles. An aqueous clay slurry with pH 10 could be readily added to the latex, while a stable colloidal latex system was still maintained. The latex eventually becomes unstable through the natural drying process at ambient temperature as films are formed. Mechanical properties were performed on dog-bone, die cut films. Attempts were made to fit the data obtained on modulus properties to theoretical models for composites.

4.2.1 Montmorillonite-reinforced rubber composite systems

Table 4.1 summarizes some of the tensile properties of the clay-filled rubber containing 5% and 10% by weight of Na-montmorillonite compared with those of unfilled rubber. Stress-strain curves are displayed in figure 4.1.

As expected the silicate reinforced systems prepared by mixing pristine montmorillonite in natural rubber latex show a superior modulus and strength relative to ordinary rubber. It is obvious that even with the addition of such a low loading of montmorillonite (5wt%-10wt%), the tensile modulus increases considerably. For example, compared to unfilled rubber, a 5 wt% clay composite has 100% higher tensile modulus and 145% higher tensile strength. Even more remarkable was the result of 10wt% clay loading which shows an increase in modulus of 500% and in tensile strength of 160%. Tensile strength improvement is apparently similar for both 5wt% and 10wt% loading whereas modulus increases as a function of clay loading. Of particular interest in this composite system is that there is no trade-off with either impact strength or toughness which is often encountered in the field of composites containing rigid fillers [1]. Toughness was determined by integrating the area under the stress-strain curve shown in figure 4.1. Composites containing 5% and 10 wt% clay have toughnesses that are twice as much as those of unfilled rubber. However, the elongation at break is observed to decrease on addition of clay filler. Generally, rigid fillers cause a dramatic decrease in elongation to break [1], whereas these present composites show only 16% and 40% loss in elongation with 5% and 10 wt% clay loading, respectively.

Properties	unfilled rubber	Na- montmorillonite	
		5% wt	10% wt
Tensile modulus (MPa)	0.01±0.001	0.02±0.002	0.06±0.009
Tensile strength (MPa)	2.8±0.1	7.1±0.5	7.5±0.7
Toughness (MPa)	10±1	20±2	20±2
Elongation at break (%)	1080±30	920±30	630±30

Table 4.1 Mechanical properties of natural rubber latex-montmorillonite composite.

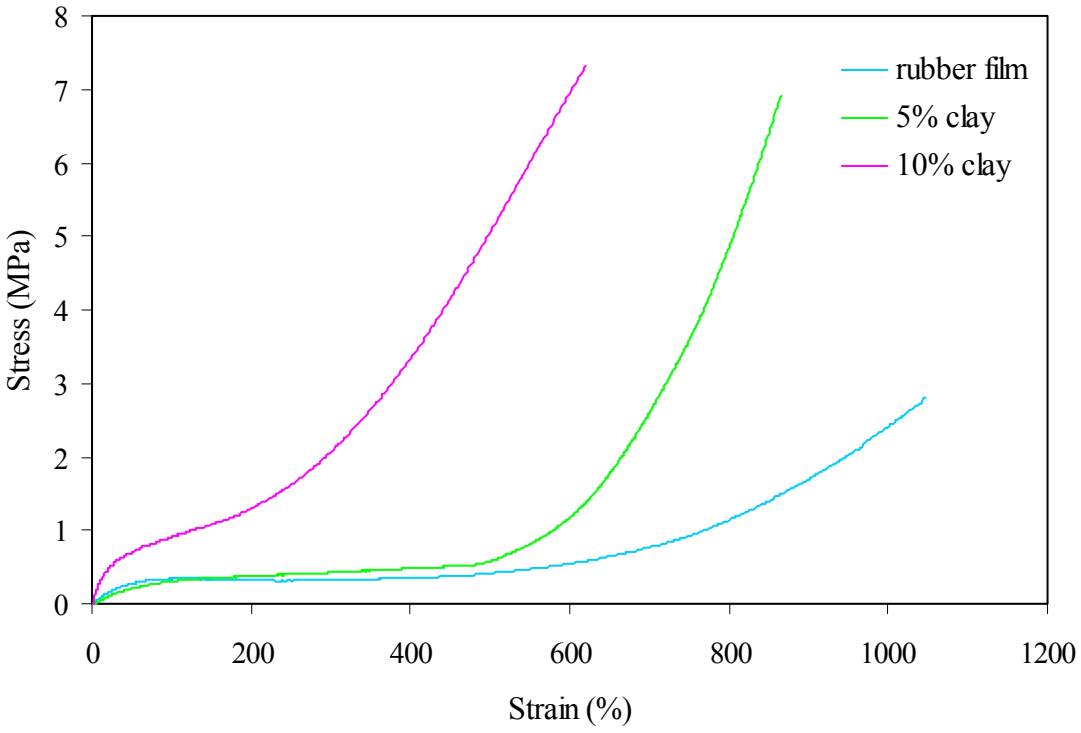

Figure 4.1 Stress-strain curves in tension of natural rubber with 5% and 10 wt% montmorillonite.

4.2.2 Kaolinite-reinforced rubber composite systems

Another filler system that was investigated is kaolinite clay which also has a platy morphology. Kaolinite has been used exclusively in natural rubber latex compounds. Depending on its particle size, kaolinite can be used as a semi-reinforcing filler (hard clay) or a non-reinforcing filler (soft clay). Hard clays contain a larger weight-percent of fine particles than do soft clays. Generally, particles less than two microns in size constitute more than 80% of hard clay weight [2]. Kaolinite particles are reported to be thin, hexagonal platelets with an aspect ratios in the range of 5:1 to 50:1 which depends on particle size [3].

Experiments were conducted to observe the reinforcement capacity of kaolinite in latex films more or less as a standard, and to compare kaolinite reinforcement to that of the montmorillonite system. Table 4.2 shows the effect of kaolinite clay on tensile properties of unvulcanized rubber film with 10% wt clay loading. Typical average responses from films containing montmorillonite at equal-weight loading are also shown as well as from rubber films containing no clay filler. Typical stress-strain curves are also displayed in figure 4.2. One can see that with the addition of kaolinite, the tensile strength, elongation at break and toughness all slightly decrease, whereas modulus is very slightly increased. Montmorillonite, on the other hand, provides vastly improved properties with the same loading. At only 10% wt of montmorillonite in the rubber, modulus increased nearly three fold and tensile strength by a factor of two. Differences between this 10% montmorillonite sample and the earlier sample reported may be due to batch to batch variations in the latex used. As noted previously of particular interest is

the improvement in toughness. The trade off between stiffness and toughness is often expected in the field of composites containing rigid fillers [1]. In contrast the montmorillonite composite systems show improved mechanical properties with virtually no sacrifice in impact toughness.

Figure 4.3 is a plot of modulus, tensile strength, toughness and % strain at break of natural rubber (NR) latex film and its mixture with kaolinite and montmorillonite. This data evidently demonstrates that, compared to neat rubber, montmorillonite offers reinforcement capacity which is far superior to kaolinite clay. Composites with montmorillonite show significant improvement in important properties such as modulus, tensile strength and toughness although these gains must be balanced against the complementary decrease in elongation. Kaolinite provides no significant effect on rubber performance at this low loading. To match the reinforcing capacity of a 10% wt montmorillonite clay composite, a significantly higher loading of kaolinite would be needed.

Properties	unfilled rubber	filled rubber (10 wt%)	
		kaolinite	Na- montmorillonite
Tensile modulus (MPa)	0.02±0.002	0.02±0.002	0.05±0.007
Tensile strength (MPa)	10±1	9±1	19±1
Toughness (MPa)	32±3	29±3	60±5
Elongation at break (%)	1080±30	1060±30	840±30

Table 4.2 Mechanical properties of natural rubber latex filled kaolinite and montmorillonite, respectively.

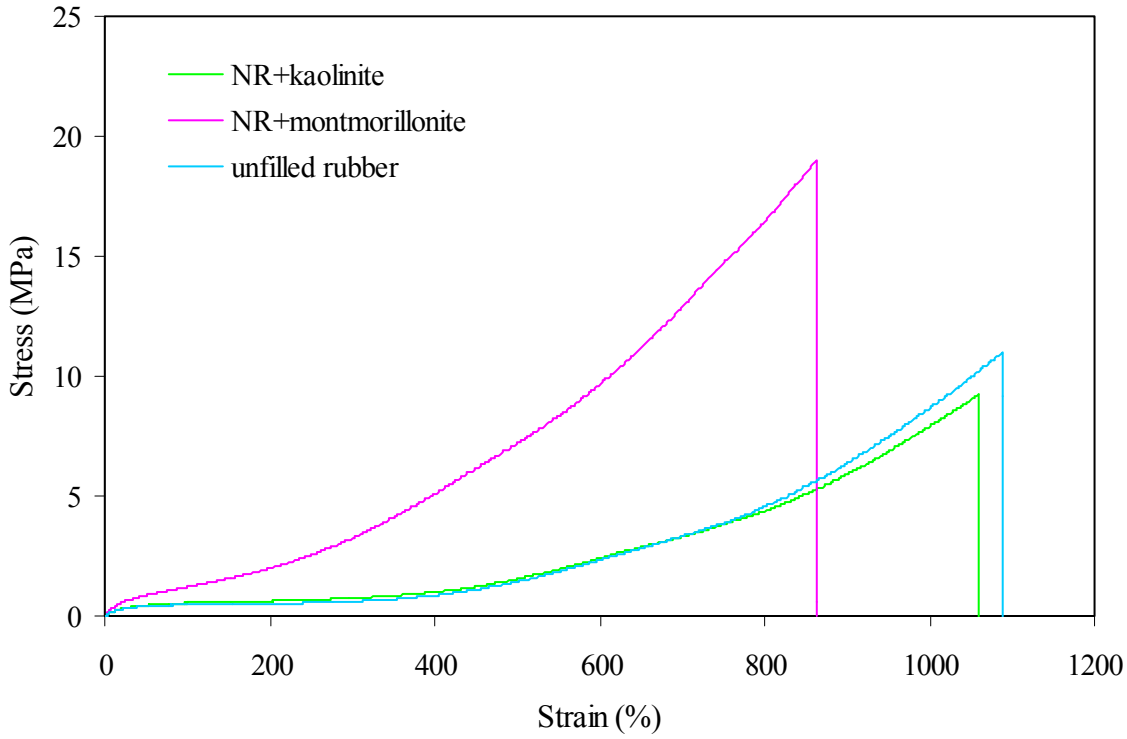

Figure 4.2 Stress-strain curves of natural rubber with 10% wt kaolinite and montmorillonite, respectively compared to the unfilled rubber.

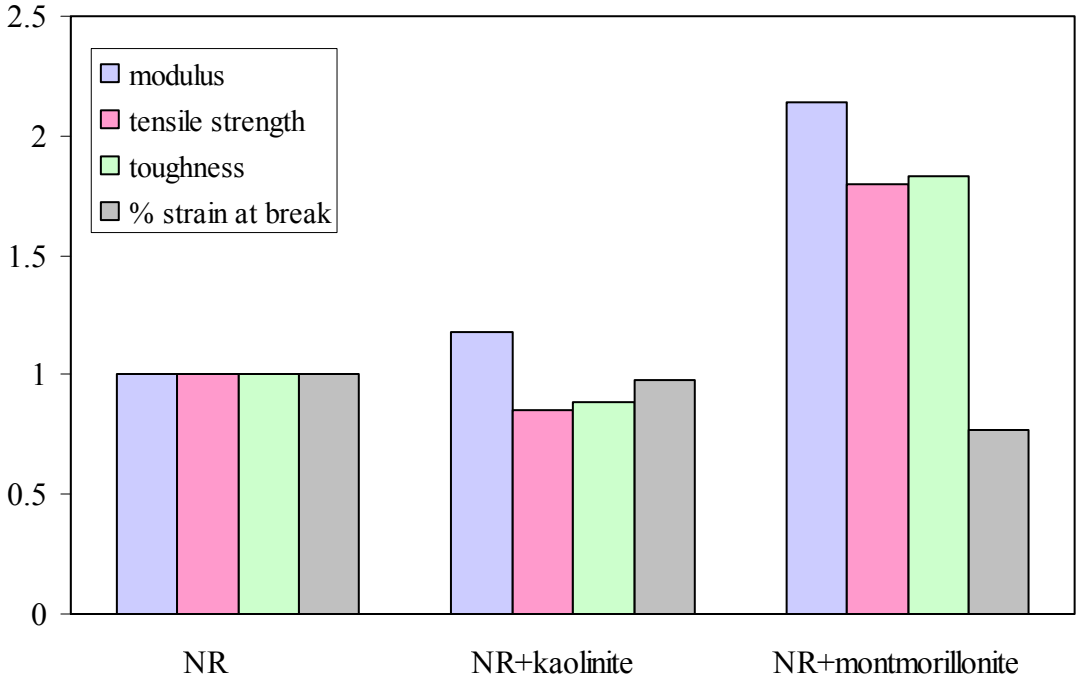

Figure 4.3 Relative Young's modulus, tensile strength, toughness, and elongation to break of 90/10 mixture of natural rubber latex with kaolinite and montmorillonite, respectively.

4.2.3 Theoretical Prediction of Composite Elastic Modulus

Composite tensile modulus has been experimentally determined as a function of composition. It is of interest to see if the experimental data fits a theoretical prediction. To compare with the theoretical model, relative moduli are plotted versus filler volume fraction and this is shown in figure 4.4.; the relative moduli of composites are defined relative to unfilled polymer. Volume fraction of inorganic material (V_f) is used to indicate the silicate loading:

$$V_f = \frac{W_{silicate}}{\rho_{silicate}} \left(\frac{1}{\frac{W_{silicate}}{\rho_{silicate}} + \frac{(1 - W_{silicate})}{\rho_{polymer}}} \right) \qquad (4.1)$$

Where:

$W_{silicate}$ is the weight fraction of silicate in the composite

$\rho_{silicate}$ is the density of montmorillonite, taken to be 2.86 g/cm^3 [4]

$\rho_{polymer}$ is the density of natural rubber latex, taken to be 0.96 g/cm^3 [5]

It can be seen from figure 4.4 that silicate reinforced composites show moduli that are higher than the unreinforced polymer. For example, a 2% volume fraction of montmorillonite exhibited an increase in Young's modulus of 100%. A very pronounced improvement in modulus can be seen with 4% volume fraction that resulted in up to 500% increase in modulus. In addition, there is a dependence of modulus on clay content, the modulus increases with an increase in clay content, but the relationship is apparently not linear.

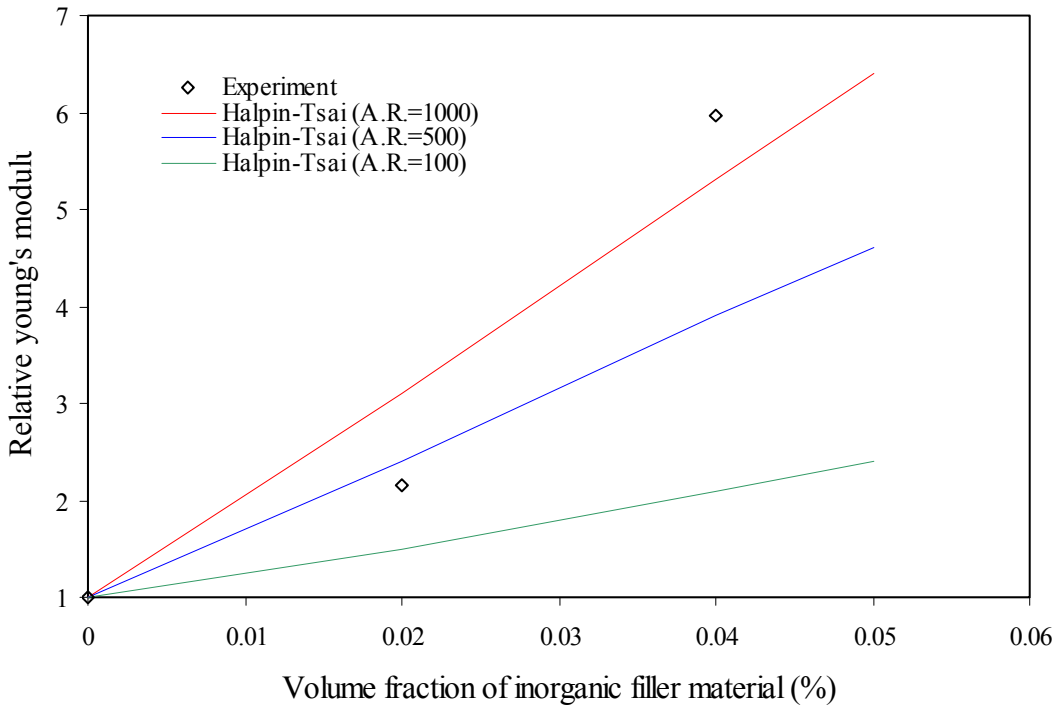

Figure 4.4 The relative Young's modulus for two natural rubber/ silicate composites. Lines are the predictions of Halpin-Tsai for various aspect ratios of fillers.

As noted in chapter 2 a large number of predictive equations describing the modulus of filled system have been developed in the literature. The simplest model is the well- known rule of mixture [6]:

$$E_{composite} = V_f E_f + (1 - V_f) E_m \quad (4.2)$$

Where:

V_f is the volume fraction of filler,

E_f and E_m is the elastic modulus of filler and matrix, respectively

This simple model indicates that the contributions of filler and matrix to the average composite properties are proportional to their volume fraction. This relationship successfully predicts behavior in particulate- filled composites, with filler aspect ratios close to 1 (spheres, cubes or blocks). It is not appropriate for highly anisotropic reinforcing materials such as flakes or platelets and fibers (needles).

Halpin and Tsai [7-10] developed a simple and generalized equation to predict moduli in fiber and flake reinforced conventional composites and this has been modified by Nielsen [11] to account for the maximum packing fraction, P_f of the filler as follow:

$$\frac{E_c}{E_m} = \frac{1 + ABV_f}{1 - B\psi V_f} \quad (4.3)$$

Where:

$$A = 1.33\left(\frac{L}{D}\right)^{0.645} \quad (4.4)$$

$$B = \frac{(E_f/E_m) - 1}{(E_f/E_m) + A} \quad (4.5)$$

$$\psi = 1 + \frac{1 - P_f}{P_f^2} V_f \quad (4.6)$$

L/D is the aspect ratio of the flakes, that is, their length divided by their thickness.

P_f is the maximum packing fraction of the platelets which varies between 0.785 and 0.907[1].

The exact value of an aspect ratio for montmorillonite is in question. Platelet-shaped montmorillonites have been reported to have thicknesses of ~1nm. Individual platelets have aspect ratios ranging from about 500:1 to 2000:1, with an average of about 1500:1[12]. Since the platelets occur naturally in stacks, those would be the effective aspect ratio expected in exfoliated systems. In the pristine state, montmorillonite is made up of stacks of platelets resulting in a much smaller aspect ratio in the range of 50-200.

As also illustrated in figure 4.4, we can see that prediction of Halpin-Tsai by first applying the aspect ratio L/D= 100 does not describe well the relative Young's modulus of both composites containing 2% and 4% volume fraction of montmorillonite. An efficient way to determine the effect of aspect ratio as a contributing reinforcement factor to the resulting relative modulus has been developed with the aid of VI software program created by Dr. Harrison. This particular Virtual Instrument allows one to predict the composite elastic modulus relative to the polymeric matrix for fiber and flake filled systems as a function of filler volume fraction and aspect ratio, and is based on Halpin-Tsai equations. The predictions for composites corresponding to L/D = 500 and 1000 are also plotted in figure 4.4. It can be seen in the case of 2 vol% of clay that in order to achieve 100% improvement in modulus, an aspect ratio of approximately 400 would be required. For 4 vol% clay loading, the predictions corresponding to aspect ratio of 1000 do a reasonable job in describing the resulting relative modulus.

According to the Halpin-Tsai theory of filler reinforcement, volume fraction and aspect ratio are key parameters governing the mechanical properties of composites. In the formation of nanocomposites, clay platelets initially stacked together to form clay particles are intercalated with polymer, exfoliated and dispersed in the polymer matrix. A single platelet layer is sheetlike, having a thickness of only about 1 nm and lateral dimensions that are typically on the order of 500-2000 nm [12]. The theoretical prediction for modulus behavior investigated above suggested that the resulting aspect ratio of 1000, with 4 vol% clay for example, is a contributing reinforcing factor. Such high aspect ratio silicate platelets could be present in exfoliated systems where individual platelets separate from the clay stack and are dispersed in the rubber matrix. In order to see if this is the case, x-ray diffraction (XRD) was conducted to explore the microstructure of natural rubber-montmorilonite composites.

It is worth noting that there are other factors that also affect rubber properties. Fillers are classified on the basis of particle size, structure and surface activity [13-17], and these parameters influence effective filler volume in ways which are not accounted for in traditional models for modulus behavior. An amount of 'bound rubber' has been reported [13] to form during mixing where rubber chain molecules become attached to filler surfaces in some way, depending on the strength of the polymer-filler interaction. This immobilized rubber portion which is physisorbed on silicate surfaces is assumed to be stiffer than bulk polymer through its affinity to the filler surfaces. In addition, the effect of filler structure on modulus (in carbon black) was also proposed [18,19] to relate to 'occluded rubber' formed. The increase in modulus observed for montmorillonite/

rubber filled systems may be due in part to a hydrodynamic effect in which the effective volume of the filler increases beyond the value calculated from its mass and density.

4.3 Structure determination by x-ray diffraction

Wide-angle x-ray diffraction (WAXD) has been used to characterize the formation and structure of polymer-silicate hybrids by monitoring the position, shape, and intensity of the basal reflection from the silicate layers. When insertion of polymer chains in the silicate layers occurs, an increase of silicate interlayer volume and corresponding layer spacing is seen which gives rise to a shift of the (001) diffraction peak to lower angles. No diffraction peaks would be visible in the case of exfoliated structures where silicate layers are completely and uniformly dispersed in a continuous polymer matrix. A broadening of the diffraction profile might indicate partial exfoliation of silicate layers as crystallite size decreases.

Figure 4.5 shows the x-ray diffraction pattern of natural rubber latex/ montmorillonite 50/50 (w/w) mixture. At the low loading used for mechanical property measurement, no WAXD diffraction is obtained for the clay. The pristine Na-montmorillonite diffraction profile is included for comparison. The 2θ values along the x- axis can be converted to layer spacing value d through the Bragg relationship ($n\lambda = 2d\sin\theta$). The characteristic basal plane spacing of montmorillonite (after Lorentz-polarization correction) occurs at $2\theta = 9.03°$ corresponding to an interlayer spacing d (001) = 9.78 Å. Whereas the x-ray diffraction pattern of the rubber/montmorillonite composite shows a slight shift to lower angles at $2\theta = 7.64°$ with a corresponding

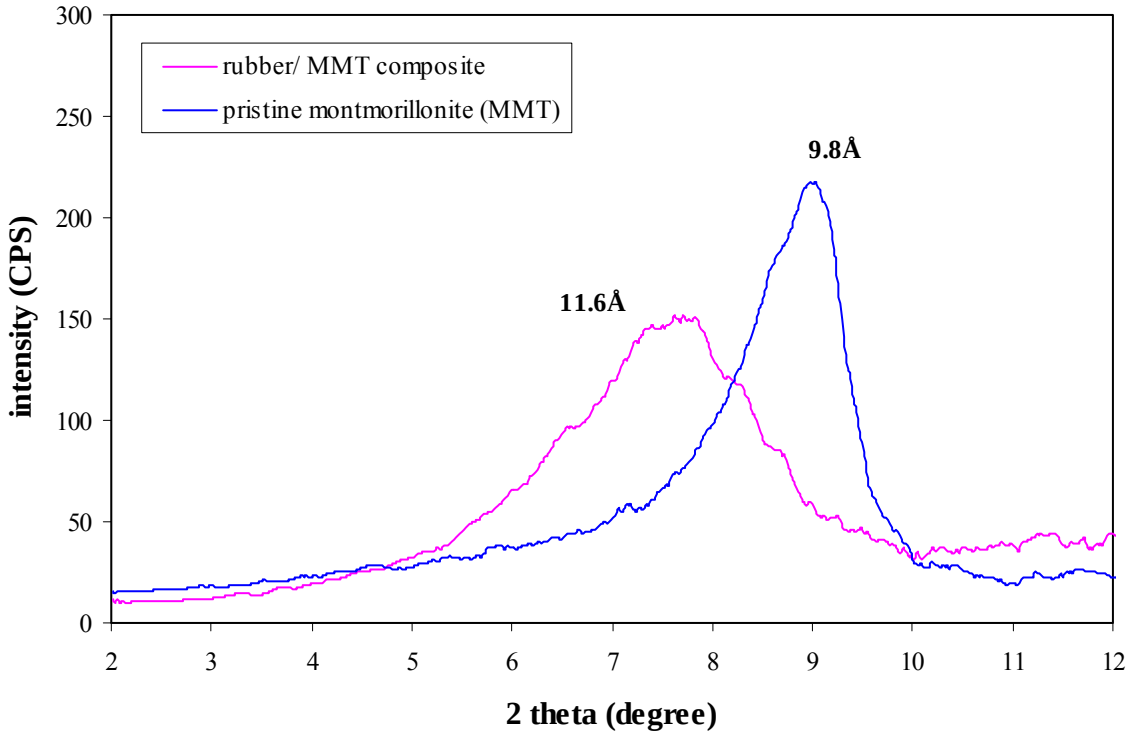

Figure 4.5 X-ray diffraction pattern of pure Na-montmorillonite (MMT) and that of the natural rubber latex/ MMT (50 wt%) composite.

interlayer distance d(001) = 11.56 Å. In addition to the increase in gallery height, an increase in breadth of the peak profile was observed. Such broadening of the diffraction peak may indicate that partial exfoliation has occurred as crystal size decrease. According to the Scherrer relation, $B = K\lambda/L\cos\theta$, where K is a numerical proportionality constant, the width of the peak B (measured by full width at half maximum, FWHM) is inversely proportional to the coherence length of the scattering entities, L and therefore reflects the coherent order of the silicate layers. As the angular width of the reflection increases, the length over which coherency exists decreases. Therefore, the observed change in FWHM of the composite suggests that the diffusion or insertion of rubbery polymer chains disrupt the layer structure of the silicate crystallite so that layers become exfoliated or more irregularly spaced from each other.

Table 4.3 summarizes the interlayer distance, apparent crystallite thickness and corresponding number of silicate layers in the crystal (N) of montmorillonite and rubber/montmorillonite composite. In order to determine the number of layers per particle, N, the breadth of the basal 001 reflection was measured and the observed diffraction widths (B(obs)) were converted into pure diffraction breadths (B) by means of the relationship $B(obs)^2 = B^2 + b^2$. A number of instrumental standard materials were used namely silver behenate, quartz, corundum and silicon. The widths from these standard materials at their appropriate diffraction angles were extrapolated and used as a measure of the instrumental broadening (b) at the appropriate angle for montmorillonite. As described by the Scherrer equation, the breadth of the reflection is proportional to the average crystal thickness, L, i.e. the mean distance perpendicular to the layers and thereby, the number of layers per particle, N which is given by L/ d(001).

	d-spacing (Å)	thickness (Å)	N
Na-montmorillonite	9.78	73.8	8
Na-montmorillonite/rubber	11.56	36.5	3

Table 4.3 Interlayer distance, stacking thickness (L) and approximate number of layers per particle (N) of pristine clay and clay/rubber composite.

In table 4.3, the basal 001 diffraction profile, after correction for the Lorentz-polarization factor and for instrumental broadening, shows that pristine Na-montmorillonite investigated is composed of crystals containing approximately N = 8 silicate layers. The silicate crystal thickness reduced remarkably with fewer structural layers (N= 3) after mixing with rubber latex suggesting possibly delamination of the stacking layered structure.

These XRD investigations reveal a broad basal 001 diffraction profile that has been shifted toward a higher interlayer spacing. The small increase in the interlayer spacing could account for some polymer intercalation, with some of the clay possibly being exfoliated into the rubber matrix.

In order to investigate whether or not the profile intensity and width increases is a function of the low concentration of montmorillonite in the composite, a series of different compositions ranging from 75%, 50% and 35% wt. mixtures were prepared and their diffraction profiles are shown in figure 4.6. Below 35% clay it is difficult to detect the 001 peak. Two diffraction bands were analyzed, namely the basal 001 diffraction and the two dimensional 11,02 diffraction peak. The two- dimensional hk peak arises from randomly stacked layers in most smectites [20]. The hk diffraction peaks of montmorillonite have been used to obtain information regarding the organization of water molecules and exchangeable cations in the hydrated forms of the minerals [21]. Analysis of the 11,02 diffraction peak showed that the intensity profile is not sensitive to structural details, e.g., changes in the organization of the exchangeable cations with hydration and of the organization of water molecules relative to the silicate layer. The intensity of 001 peaks were then measured relative to the intensity of 11,02 peaks (which is taken as a measure of the total amount of silicate in the beam), these peak ratios are shown in table 4.4. Within experimental error, the lack of a consistent trend in the relative intensity measured versus clay concentration suggests that the increase in 001 profile width is not an artifact of the lower concentration of clay in the mixture but represents a real physical change in the particle. Further the low value of 001 peak intensity versus 11,02 at 35% clay might suggest that some of the clay is no longer present in stacks, i.e. it has been exfoliated.

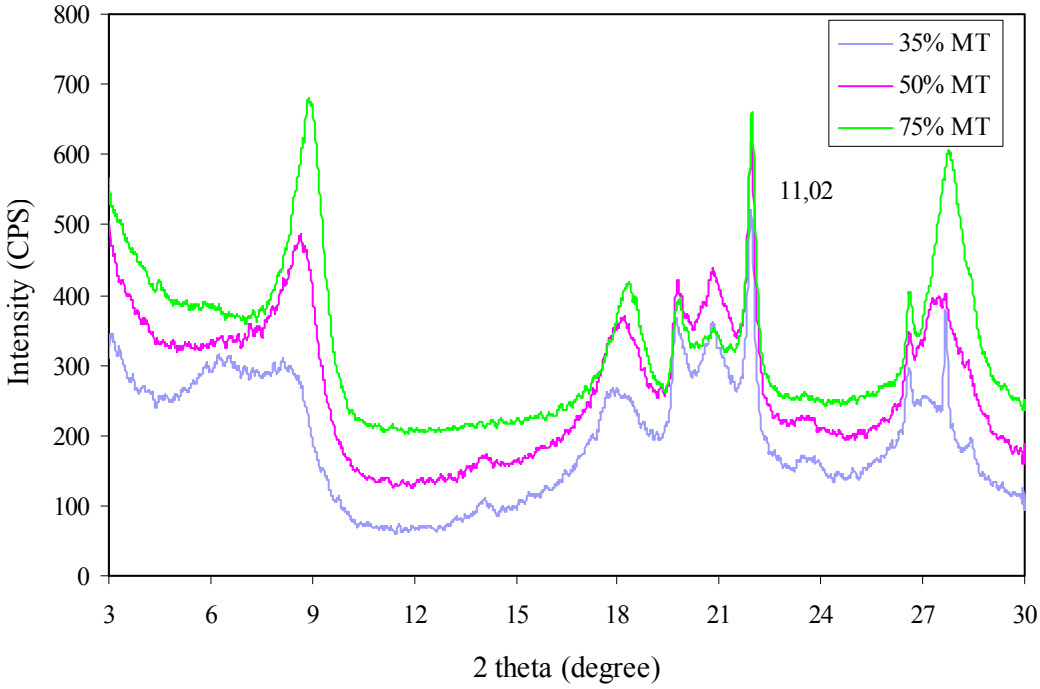

Figure 4.6 X-ray diffraction pattern of natural rubber/clay composite containing 35%, 50%, and 75% weight of montmorillonite respectively.

Clay composition	Relative intensity vs. 11,02
35%wt	0.65
50%wt	0.83
75%wt	0.75

Table 4.4 The relative intensity of mixtures at different clay concentrations.

4.4 Water vapor permeability study

Water vapor permeability of polymer nanocomposites have been studied by several workers owing to the interest in developing polymer materials with improved barrier properties. Polyimide- hybrid with montmorillonite was reported to show excellent gas barrier properties although water vapor barrier properties have not shown corresponding improvements [22]. In contrast the water vapor permeability of poly (ε-caprolactone) nanocomposites were shown to be reduced dramatically due to dispersion of impermeable high aspect ratio silicate layers within the polymer matrix [23].

Figure 4.7 shows a plot of the amount of ***water uptake*** versus exposure time for a composite film containing 2% vol. fraction of inorganic silicate. These plots were subsequently used to calculate water vapor transmission rate and water permeability. Higher levels of clay were not used because of problems in ensuring that good "pin-hole" free films could be produced.

According to ASTM E96- 95, *water vapor transmission rate* (WVT) is defined as the steady water vapor flow in unit time through unit area of a body, normal to specific parallel surfaces, under specific conditions of temperature and humidity at each surface.

$$WVT = (G/t) / A \qquad (4.7)$$

Where

G = weight change, g

t = time, h

A = test area (cup mouth area), m^2 and

WVT = rate of water vapor transmission, g/h· m^2

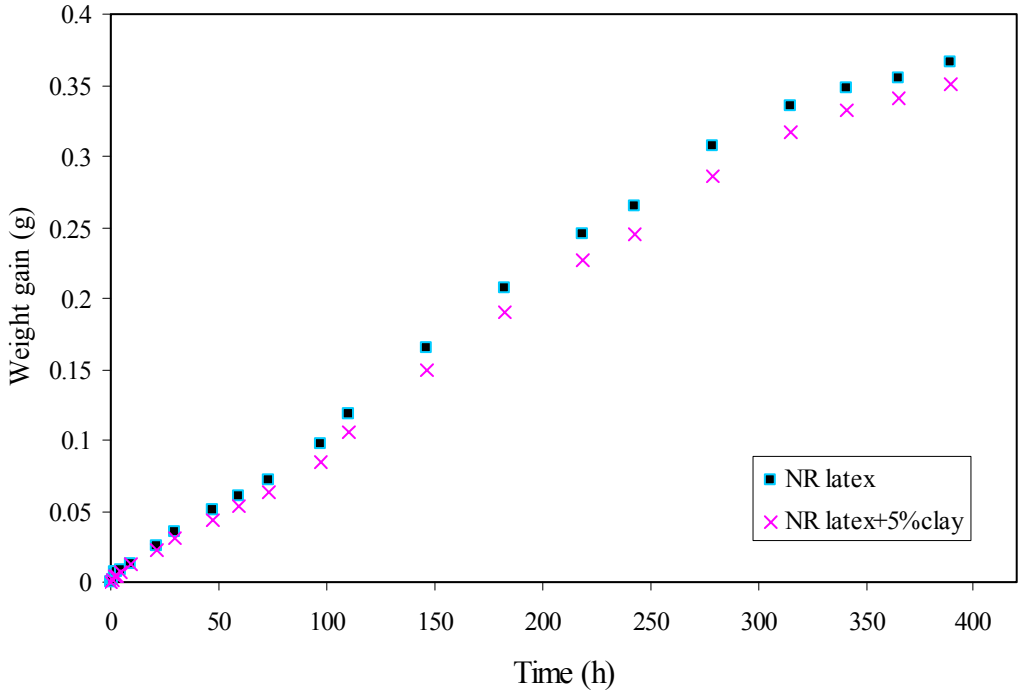

Figure 4.7 Water weight gain of composite film containing 5 wt% montmorillonite versus exposure time.

Water vapor permeance is the time rate of water vapor transmission through unit area of flat material induced by unit vapor pressure difference between two specific surfaces, under specific temperature and humidity conditions.

$$\text{Permeance} = \text{WVT} / \Delta p \qquad (4.8)$$

Where

Δp = vapor pressure difference, Pa.

The relative permeability of the composite film will be the permeability of the composite film divided by the permeability of the natural rubber film. Therefore, the calculated value for relative permeability of the composite is 0.93. This means that a 2% volume fraction (5 wt%) of montmorillonite decreased the permeability of rubber film to water by ≈ 7% which doesn't constitute a significant change relative to natural rubber. This lack of significant improvement may be due to the fact that a completely oriented layered structure parallel to the film surface and uniformly dispersed system is very difficult to achieve experimentally.

4.5 PMMA-grafted natural rubber/ clay composite

A graft-copolymer of natural rubber latex and methyl methacrylate come to our attention as another polymer matrix that may be of interest due to its increased polar characteristics. These graft copolymers are basically elastomers which have been modified by graft-copolymerization with a reinforcing resin. They are made by polymerizing methyl methacrylate monomer in the presence of natural rubber latex whereby polymethylmethacrylate (PMMA) chains are grafted to the rubber molecules [2, 24]. These materials are available commercially under the general trade name of Heveaplus MG. There has been a small but consistent demand for this graft-copolymer for applications which require a hard rubber with optimum retention of properties such as tensile strength and impact strength, and where black compounds are undesirable [25]. When blended with normal latex, improvements in modulus and tear have been reported [26].

PMMA-layered silicate nanocomposites have been reported to be synthesized via in situ free radical polymerization [27-28]. A composite intercalated with PMMA was obtained by an emulsion polymerization in which MMA comonomer is dispersed in a water phase and polymerized with a water soluble radical initiator in the presence of Na^+-montmorillonite, without employing any further modification of the monomer or without the addition of any coupling agents. Ion-dipole interactions are believed to be the driving force for the introduction and fixation of the organic polymer chains lying flat on the layer silicate surface.

The PMMA-grafted natural rubber/clay composites studied were prepared by the same procedure as previously described for normal natural rubber/clay composites. The grafted latex sample contains 30% of PMMA with a total solids content of 50±1.5%. An aqueous solution of sodium montmorillonite was added to the grafted rubber latex. Films were cast by drying the solution at 25°C. Ground films were subsequently pressed into pellets for XRD analysis.

Figure 4.8 illustrates the XRD pattern of grafted rubber /clay (50/50 w/w) composite including profiles of pristine montmorillonite and that of the 'unmodified' normal rubber/ clay composite. The x-ray diffraction pattern of the grafted rubber mixture has a reflection with an identical 2θ position and d-spacing as that of the original rubber latex/clay mixture, and has a broad 001 diffraction peak with a small increase in the interlayer spacing. The polar character of the methacrylate ester containing a –CO-O- functional unit was expected to have improved its dispersion with the polar surfaces of the silicates and make more amenable to penetration into the clay galleries. However, based on the observed diffraction profile this does not seem to be the case in this system.

Similarities between the behavior observed in XRD for normal rubber and grafted rubber composite systems indicate that some polymer intercalation occurs probably together with partial exfoliation. Moreover, the enhanced modulus and strength properties observed earlier reflect a direct result of the polymer-clay filler bonding. Physical Van der Waals attraction between rubber segments and clay surfaces may play a part in the overall adhesion process.

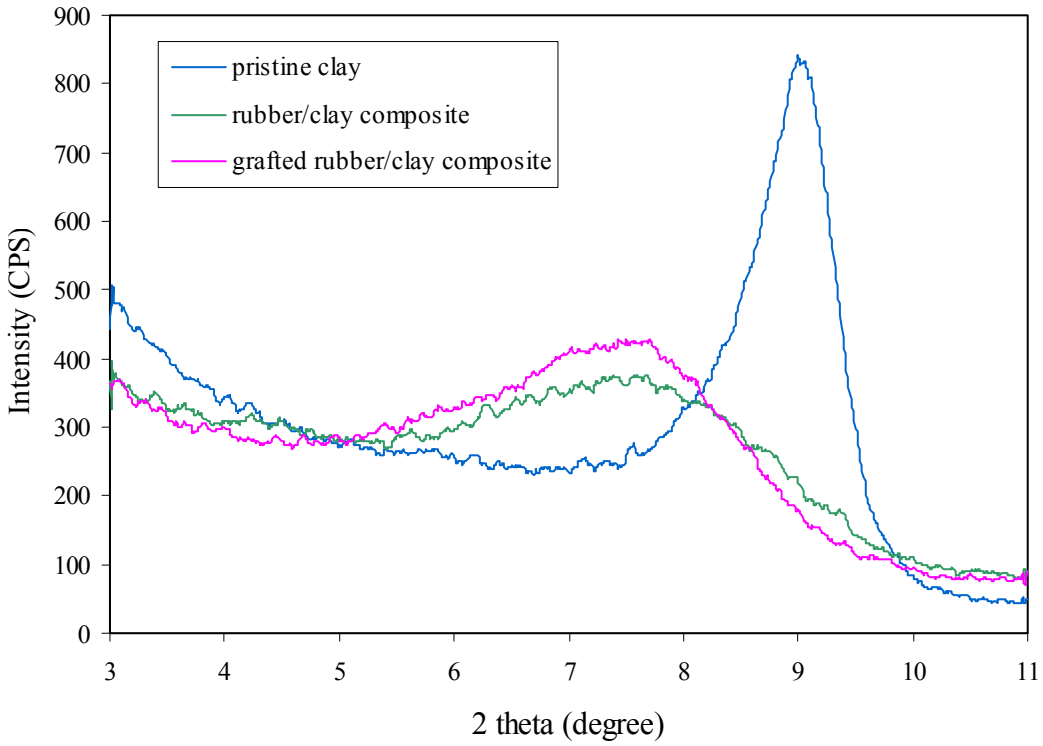

Figure 4.8 X-ray diffraction patterns of PMMA-grafted natural rubber/clay composite, Pristine Na^{+}- montmorillonite and natural rubber/clay composite.

REFERENCES

1. Nielsen, L. E. and Landel, R. F. (1994) Mechanical Properties of Polymers and Composites, 2 nd ed, Marcel Dekker, Inc., 545 pp.
2. Morton, M., Editor (1987) Rubber Technology, 3 ed., Van Nostrand Reinhold Co., New York, 631 pp.
3. Rothon, R., Editor (1995) Particulate-Filled Polymer Composites, Longman Scientific & Technical, New York, 371 pp.
4. Material Data Sheet: Southern Clay Products, Inc., Gonzales, Texas.
5. Brandrup, J. and Immergut, E. H. (1975), Polymer Handbook, 2 nd. ed., John Wiley& Sons, New York.
6. Agarwal, B. D. and Broutman, L. J. (1990), Analysis and Performance of Fiber Composites, 2 nd. ed., Wilet, New York, 448 pp.
7. Halpin, J. C. (1969), Stiffness and Expansion Estimate for Oriented Short Fiber Composites, J. Composite Materials, 3, 732.
8. Halpin, J. C. (1969), Primer on Composite Materials Analysis, 2 nd. ed, Technomic, Lancaster, Pa., 227 pp.
9. Halpin, J. C. and Kardos, J. L. (1976), The Halpin-Tsai Equation: A Review, Polymer Eng. Sci., 16(5), 344.
10. Tsai, S. W. (1968), Formulus for the Elastic Properties of Fiber-reinforced Composites, U. S. Dept. Commerce Rept. AD834851.
11. Nielsen, L. E. (1970), Generalized Equation for the Elastic Moduli of Composite Materials, J. of Applied Physics, 41(11), 4626.

12. Miller, B. (1997) “Nano Clay Particles Create New Compound”, Plastics Formulating & Compounding, 3, 30-32.
13. Blow, C. M. (1971) Rubber Technology and Manufacture, The Chemical Rubber Company, 509pp.
14. Wang, M. J. (1998) “Effect of Polymer-Filler and Filler-Filler Interactions on Dynamic Properties of Filled Vulcanizates”, Rubb Chem Technol, 71, 520-583.
15. Donnet, J. B. (1998) “Black and White Fillers and Tire Compound”, Rubb Chem Technol, 71, 323-339.
16. Wang, M. J., Wolff, S. and Tan, E. W. (1993) “Filler-Elastomer Interactions; Part VIII the Role of the Distance between Filler Aggregates in the Dynamic Properties of Filled Vulcanizates”, Rubb Chem Technol, 66, 178-195.
17. Wolff, S. (1990) “Characterization of Fillers in Vulcanizates According to the Einstein-Guth-Gold Equation”, Rubb Chem Technol, 63, 32-45.
18. Medalia, A. J. (1987) “Effect of Carbon Black on Ultimate Properties of Rubber Vulcanizates”, Rubb Chem Technol, 60, 45-61.
19. Medalia, A. J. (1972) “Effective Degree of Immobilization of Rubber Occluded within Carbon Black Aggregates”, Rubb Chem Technol, 45, 1171-1194.
20. Brindley, G. W., and Brown, G. (1980) Crystal Structure of Clay Minerals and their X-ray Identification, Mineralogical Society, 485 pp.
21. Mering, J. and Brindley, G. W. (1967) “X-ray Diffraction Band Profiles of Montmorillonite- Influence of Hydration and of the Exchangeable Cations”, Clay clay minerals, 15, 51-60.

22. Yano, K. et al (1993) “Synthesis and Properties of Polyimide-Clay Hybrid”, J. of polymer sci: Part A: polymer chemistry, 31, 2493-2498.
23. Messersmith, P. B. and Giannelis, E. P. (1995) “Synthesis and Barrier Properties of Poly(ε- caprolactone)-Layers Silicate Nanocomposites”, J. of polymer sci: Part A: polymer chemistry, 33, 1047-1057.
24. Indian Rubber Institute (2000), Rubber Engineering, McGraw Hill, 901 pp.
25. Blackley, D. C. (1966) High Polymer Lattices; Their Science and Technology: Volume 1 Fundamental Principles, Palmerton Publishing Co., New york, 351 pp.
26. Poh, W. N. (1989) Development in Natural Rubber Latex: Production, Properties, Stability, Elastomerics, 121, 9-15.
27. Lee, D. C. and Jang, L. W. (1996) Preparation and Characterization of PMMA- Clay Hybrid Composite by Emulsion Polymerization, J. of Appl. Polym. Sci., 61,1117-1122.
28. Huang, X. and Brittain, W. J. (2001) Synthesis and Characterization of PMMA Nanocomposite by Suspension and Emulsion Polymerization, Macromolecules, 34, 3255-3260.

CHAPTER 5

5.1 Conclusion

Composites formed from of natural rubber with layered silicates as the inorganic phase reinforcement were studied. Their preparation involves mixing the layered silicate with rubber in the latex (water medium) form where clay can be readily dispersed without causing the latex to coagulate; the two components apparently mixed and dispersed uniformly. The resulting polymer composites exhibit a dramatic improvement in mechanical properties compared to neat rubber and the conventional kaolinite- reinforced rubber. Of particular interest is that such composites enhance important properties like modulus and tensile strength with virtually no sacrifice in impact strength and toughness, which is typically encountered with rubber-reinforced systems where filler particles are micron sized. This reinforcing effect has been discussed with regard to a theoretical model of composite modulus (Halpin-Tsai). It was suggested that the reinforcing potential observed could be attributed to an aspect ratio as high as 400-1000 for the dispersed silicate layers. Clay is apparently dispersed into individual platelets in the rubber matrix while rubber molecules intercalate to the clay galleries. XRD results suggested evidence for delamination of the stacking layered structure but not complete exfoliation. The splitting of clay clusters into individual platelets leads to the formation of high aspect ratio silicate layers with nanometer thicknesses. These nano particles dispersed in the rubber latex system are presumably the key to producing composite with the observed enhanced properties.

We speculate that the driving force for the adsorption process which promotes interaction between hydrophilic silicate layer and the rubber hydrocarbon particles in this latex system studied is entropic. Layer silicates, owing to the weak forces that stack the layers together, can be readily dispersed in the watery latex phase, which leads to the insertion of rubber molecules into the silicate interlayer galleries. The adsorption of polymer onto the delaminated sheets may be ascribed to the van der Waal forces between rubber segments and the clay surface. These secondary interactions then become significant when the clay-rubber complex is allowed to dry out; clay sheets may partially reassemble to stacks with fewer layers than originally present but some isolated silicate layers act to reinforce the rubber matrix.

5.2 Future Work

The reinforcing ability of a nanoscale dispersed layer silicate in natural rubber (polyisoprene) latex has been demonstrated. The observed improvement in modulus and tensile strength reflects evidence of the interfacial bonding between the rubber matrix and silicate particles. An increased modulus presumably occurs as a direct result of attachment of rubber to the clay filler, which has the effect of reducing polymer mobility. In the absence of strong coupling bonds, polymers are physically adsorbed on the surface of the clay, resulting in a decreased mobility of rubber molecules near the surface of the clay. Van der Waal forces are presumably responsible for the adsorption of rubber segments onto delaminated silicate sheets. Weak interfacial bonding and possible particle aggregation of montmorillonite may be responsible in part for the decrease in

elongation at break observed in the resulting composites. Dewetting, or the breaking of aggregates, could occur since the matrix is restricted in its ability to stretch between packed particles.

The compatibility of clay platelets with the rubber organic phase, in terms of wetting and dispersion, may be substantially improved by, for instances, the covalent addition of some organics to the reactive surface of the clay. Organosilane coupling agents may be used to help the dispersion and to improve clay-rubber adhesion.

In a number of polymer/clay systems, interaction is improved by organically modifying the clay surface. This procedure does not work for latex systems since the organically modified clay surface is typically more hydrophobic to make it more compatible with the typically non-polar polymer. However, it may be possible to find a combination of organoclay and appropriate water soluble surfactant to improve the overall dispersion.

VITA

Rattana Tantatherdtam was born on August 10, 1972 in Bangkok, Thailand. In 1994, she received a B. S. degree in Industrial Chemistry from Srinakarinwirot University, Bangkok. During her Master work in 1995 at King Mongkut Institute of Technology Thonburi, she was granted a scholarship from the Royal Thai Government and was enrolled as a graduate student in Polymer Science program at the Pennsylvania State University. She received her M. S. degree in Materials Science and Engineering in December 1999. She was subsequently awarded for Ph. D. in Materials Science and Engineering (polymer option) in August 2003.